

# Journal of Materials Chemistry A

Accepted Manuscript



This is an *Accepted Manuscript*, which has been through the Royal Society of Chemistry peer review process and has been accepted for publication.

*Accepted Manuscripts* are published online shortly after acceptance, before technical editing, formatting and proof reading. Using this free service, authors can make their results available to the community, in citable form, before we publish the edited article. We will replace this *Accepted Manuscript* with the edited and formatted *Advance Article* as soon as it is available.

You can find more information about *Accepted Manuscripts* in the [Information for Authors](#).

Please note that technical editing may introduce minor changes to the text and/or graphics, which may alter content. The journal's standard [Terms & Conditions](#) and the [Ethical guidelines](#) still apply. In no event shall the Royal Society of Chemistry be held responsible for any errors or omissions in this *Accepted Manuscript* or any consequences arising from the use of any information it contains.

# Functionalized mesoporous structured inorganic materials as high temperature proton exchange membranes for fuel cells

San Ping Jiang

Fuels and Energy Technology Institute & Department of Chemical Engineering

Cxurtin University, Perth, WA 6102, Australia

## CONTENTS

Abstract.....	2
1. Introduction.....	3
2. Overview of the high temperature proton conductor materials .....	5
3. Functionalized inorganic mesoporous proton conductors .....	7
3.1. TiO <sub>2</sub> .....	7
3.2. Silica and silica based glass .....	8
3.3. Al <sub>2</sub> O <sub>3</sub> and other ceramic materials.....	14
4. Heteropolyacids functionalized mesoporous silica.....	15
4.1 Synthesis of HPW functionalized mesoporous silica nanocomposites.....	16
4.2 Microstructure, conductivity and performance.....	18
4.2.1 Microstructure.....	18
4.2.2 Conductivity and cell performance.....	20
4.3 Proton hopping within HPW-meso-silica nanocomposite.....	23
5. Prospect of functionalized mesoporous silica for high temperature PEMFCs .....	24
Acknowledgement .....	30
References:.....	30

## Abstract

There are significant technological and economical advantages for operating a proton exchange membrane fuel cell (PEMFC) at temperatures above 100-150°C. One of the key components in the development of high temperature PEMFCs is the proton exchange membrane (PEM). The PEM not only needs to be highly stable in the harsh chemical and physical environment in fuel cells, but also possesses the high proton conductivity at elevated temperatures and low humidity conditions. In this paper, the research activity and progresses in the development of high temperature PEM will be briefly reviewed but the main emphasis will be on the development of unsupported and functionalized nano and mesoporous structured inorganic materials such as TiO<sub>2</sub>, Fe<sub>2</sub>O<sub>3</sub>, Al<sub>2</sub>O<sub>3</sub> and SiO<sub>2</sub> as high temperature PEMs for fuel cells. Among various inorganic proton conducting materials, heteropolyacids (e.g., H<sub>3</sub>PW<sub>12</sub>O<sub>40</sub> or HPW) functionalized mesoporous silica, HPW-*meso*-silica, shows particular promising potential as new PEMs for fuel cells. The challenge and prospect of the development of functionalized mesoporous silica based PEMs for fuel cells operated at high temperatures (300-450°C) is discussed.

## 1. Introduction

Among various fuel cells, proton exchange membrane fuel cells (PEMFCs), where chemical energy of fuels such as hydrogen, methanol and ethanol is directly converted to electrical energy, provide an efficient alternative to standard internal combustion engines and are most suitable for applications ranging from portable electronic devices, vehicle transportation to stationary power generation.<sup>1-3</sup> PEMFCs have the advantages of high power densities, very low greenhouse gas emissions, low-temperature operation, rapid start-up and shut-down times, the ability to use fuels from renewable sources, compact design and lightweight.<sup>4-6</sup>

One of the key components in a fuel cell system is the proton exchange membrane (PEM). The state-of-the-art PEM is the perfluorosulfonic acid (PFSA) based polymers like Nafion due to their good mechanical properties, excellent chemical and physical stability and relatively high proton conductivity at fully hydrated conditions.<sup>7, 8</sup> However, the water uptake and consequently the proton conductivity of PFSA-based membranes decrease considerably at elevated temperatures ( $\geq 100^\circ\text{C}$ ) due to the dehydration and degradation of the membranes over  $100^\circ\text{C}$  and at low relative humidity (RH) environment.<sup>9-13</sup> This loss of conductivity is related to their inability to retain water at high temperatures. The limited operating temperature range complicates water and heat management, requires high-purity hydrogen to avoid CO poisoning of the catalysts and slows the electrochemical reactions at electrode/membrane interfaces.<sup>14-16</sup> Polymeric membranes are also susceptible to deformation due to the volumetric changes on the basis of adsorption/desorption of water. The deformation increases the electrode/membrane interface resistance and decreases the fuel cell performance.

Increasing the operating temperatures of PEMFCs above 100 °C has significant advantages over conventional room temperature PEM fuel cells and is one of the growing important research areas in fuel cells.<sup>15-20</sup> This includes:<sup>15, 16, 21</sup> (i) Operation at elevated high temperatures substantially enhances the catalytic activity of the electrocatalysts for the O<sub>2</sub> reduction and oxidation reactions of fuels such as hydrogen, methanol and ethanol; (ii) CO tolerance of the catalysts is drastically increased, allowing the use of lower quality reformed hydrogen; (iii) The heat and water management is substantially simplified due to existence of single water phase and the increased temperature gradient between the fuel cell stack and the coolant; and (iv) waste heat can be recovered as a practical energy source. Direct alcohol fuel cells (DAFCs) also benefit significantly from the increased operation temperatures.<sup>6, 22, 23</sup>

There are extensive research efforts and activities in the development of alternative proton exchange membranes (PEMs) with adequate performance at intermediate temperatures from 100 to 200°C.<sup>20, 24-28</sup> In particular the development of all inorganic materials based proton conductor with conductivities greater than 10<sup>-2</sup> Scm<sup>-1</sup> in the temperature range of 200-400°C under low water content is most attractive for the high performance direct liquid fuels based fuel cells. A number of biofuels can be directly oxidized or reformed to hydrogen *via* an internal reformer in this temperature range. The operating temperature is also high enough to permit the use of non-precious metal based catalysts with substantially reduced cost for fuel cells. This paper will start with an overview on the progress and achievement on the current high temperature PEMs. And the main focus of the paper will be on the development of nanoporous and mesoporous structured inorganic materials as the new class high temperature PEMs for fuel cells.

## 2. Overview of the high temperature proton conductor materials

One way to enhance the operation temperature of conventional PEMs is to develop composite membranes with polymeric matrix and inorganic proton conductive fillers. The inorganic fillers are expected to sequester water and act as a better proton conductor at higher temperature than the pure polymeric membrane. Inorganic metal oxides,<sup>29-33</sup> heteropolyacids,<sup>34-36</sup> mesoporous materials,<sup>33, 37, 38</sup> zeolites<sup>39, 40</sup> and layered, metal phosphates and phosphonates<sup>41</sup> have been used as fillers in composite membranes. Although some of the composite membranes show improved conductivity above 100°C, they still function better at high RH and also suffers reduced durability due to the additional phase boundaries between the polymeric matrix and inorganic fillers.<sup>42</sup>

Phosphoric acid doped polybenzimidazole (PBI/PA) has been shown to be a promising candidate for high temperature proton conductive material.<sup>43</sup> With the characterization of self-ionization and self-dehydration, phosphoric acid doped PBI can operate at low relative humidity and elevated high temperatures as compared to Nafion<sup>®</sup> membranes. Proton conductivities are found to be dependent on the acid doping level, RH and temperature. A conductivity of  $6.8 \times 10^{-2} \text{ Scm}^{-1}$  is reported for PBI membranes with a PA doping level of 5.6 ( $\text{H}_3\text{PO}_4$  per repeat unit of PBI) at 200°C and 5% RH.<sup>43</sup> Xiao et al.<sup>44, 45</sup> synthesized pyridine-based PBI, using polyphosphoric acid (PPA) as both solvent and polycondensation agent, achieving a high proton conductivity of  $\sim 0.2 \text{ Scm}^{-1}$  at 200°C. Though PBI/PA PEM fuel cells can run under temperatures from 120 °C to 200 °C, leaching of phosphoric acids during operation is still a significant issue. According to Savadogo and Xing,<sup>46</sup> after working for 125 minutes, the current density of phosphoric acid-polymer electrolyte decreased to  $\sim 60\%$  of the original as a result of the flushing function of the water generated during the fuel cell operation. Another problem is the chemical stability of polymer matrix. After exposed at relatively low temperatures of 68 °C for 30

minutes, structural damage appeared in the PBI matrix due to free radicals attack with the existence of  $\text{H}_2\text{O}_2$  and  $\text{Fe}^{2+}$ .<sup>47</sup>

Inorganic solid acid composites, such as  $\text{CsHSO}_4$ ,  $\text{CsH}_2\text{PO}_4$  and their derivations have drawn considerable attention due to their superprotonic properties under operating temperatures ranging from 100~300 °C.<sup>25, 48</sup> Thermal stability, conductivity at ambient pressure and high pressure of  $\text{CsH}_2\text{PO}_4$  have been studied by Boysen *et al.*<sup>49</sup> The results show that the phase transition occurs at  $228\pm 2$  °C and the conductivity increases sharply above this temperature. The strong dependence of solid acid compounds on phase transition temperature severely restrict their practical application in PEMFCs as a result of the difficult start for PEMFCs under low temperatures (<100 °C). The stability of the solid acid in a fuel cell environment is also an issue.<sup>50</sup> To improve the stability of the solid acids, Yamane *et al.*<sup>51</sup> prepared solid solutions of  $(\text{CsHSO}_4)_{1-x}(\text{CsH}_2\text{PO}_4)_x$  ( $x=0.25-0.75$ ) by a mechanical milling method. The composites were shown to have a superprotonic phase between 20 and 147 °C for  $0.25\leq x\leq 0.75$ . However, the stability of these composites depends not only on the composition, but also on the relative humidity.

Different from the oxyanions contained solid acid compounds, metal diphosphate compounds, one of the derivations of phosphoric acid composites, show proton conductivity which is free from the dependence on phase transition.<sup>24</sup> A possible candidate is the ammonium polyphosphate,  $\text{NH}_4\text{PO}_3$ .<sup>52</sup> However, pure ammonium polyphosphate is not stable at temperature higher than 200°C. Sun and Stimming<sup>53</sup> studied the proton conductivity properties of  $\text{SiO}_2\text{-TiO}_2\text{-NH}_4\text{PO}_3$  composite prepared by sol-gel method. The addition of  $\text{TiO}_2$  and  $\text{SiO}_2$  increased the proton conductivity and the best results were obtained on the composite with 10 mol %  $\text{TiO}_2$ ,  $0.043\text{ Scm}^{-1}$  at 225°C under humidified hydrogen. Hibino *et al.*<sup>54</sup> reported the considerably high proton conductivity of In<sup>3+</sup>-doped  $\text{SnP}_2\text{O}_7$  ( $\text{Sn}_{0.9}\text{In}_{0.1}\text{P}_2\text{O}_7$ ),  $0.1\text{ S}\cdot\text{cm}^{-1}$  in the temperature range from 150

°C to 350 °C under unhumidified conditions. Huang et al.<sup>27, 55</sup> studied the proton conductivity properties of niobium and indium doped niobium phosphates. Niobium phosphates show a high proton conductivity of  $1.6 \times 10^{-2} \text{ Scm}^{-1}$  at 250°C in dry air and indium doping slightly improves the conductivity. The niobium phosphate based cells show stable open circuit potential of 0.863 V at 200°C.<sup>27</sup>

For readers interested in the development and technological challenges of inorganic/organic hybrid materials, PBI/PA composite, metal diphosphate compounds, solid acid compounds and alternative polymeric membranes such as sulfonated PEEK-based polymers as potential high temperature PEMs for fuel cells, various reviews are available.<sup>15, 20, 24, 56-60</sup> In following sections, the emphasis will be on the development and potential application of the inorganic materials with meso or nanoporous structures as PEMs for fuel cells.

### 3. Functionalized inorganic mesoporous proton conductors

#### 3.1. $\text{TiO}_2$

Highly ordered mesoporous  $\text{TiO}_2$  with uniform pore size ( $\sim 7.6 \text{ nm}$ ) and high surface area ( $271 \text{ m}^2 \text{ g}^{-1}$ ) can be synthesized using titanium isopropoxide as a titania source and triblock copolymer P123 as a template.<sup>61</sup> Titanium (IV) oxides of various degrees of hydration,  $\text{TiO}_2$ ,<sup>62-65</sup>  $\text{H}_2\text{Ti}_3\text{O}_7$ <sup>66</sup> and  $\text{H}_2\text{Ti}_4\text{O}_9$ ,<sup>67</sup> have been shown to conduct protons from room temperature to 150°C. It has been known that the surface of  $\text{TiO}_2$  has both Lewis acid (five-coordinated  $\text{Ti}^{4+}$  ions) and basic (two-coordinated  $\text{O}^{2-}$ ) sites. Water can be adsorbed on the five-coordinated  $\text{Ti}^{4+}$  ions in a molecular and/or in a dissociated form.<sup>68</sup> Vichi et al.<sup>62, 63</sup> investigated the protonic conductivity in a mesoporous  $\text{TiO}_2$  membrane as a function of surface chemistry. Changing the surface site density (number of water molecules per square nanometer) from 5.5 to 5.7 leads to an increase in



conductivity from  $8.00 \times 10^{-3}$  to  $1.00 \times 10^{-2}$  S cm<sup>-1</sup> at 25 °C and 81% RH. The results indicate that values in proton conductivity do not totally correlate with the water content in these materials, indicating that surface chemistry strongly affects the water uptake and proton conductivity of the nano-porous TiO<sub>2</sub>. Further studies show that proton conductivity and water uptake of nanoporous TiO<sub>2</sub> is also affected by the pore structure (e.g., porosity, pore size and surface).<sup>69</sup>

Colomer<sup>70</sup> synthesized mesoporous TiO<sub>2</sub> thin film on glass substrates by a sol-gel technique. The films are mesoporous with an average pore diameter of 5.8 nm and the results show the conductivity improves with the increasing RH, exhibiting a sharp change at ~60%RH (see **Figure 1**). The maximum conductivity is  $8.71 \times 10^{-3}$  Scm<sup>-1</sup> at room temperature and 81% RH and  $3.78 \times 10^{-2}$  Scm<sup>-1</sup> at 80°C and 81% RH with activation energy of 0.23-0.37 eV.<sup>70</sup> Low conductivity in the range of  $10^{-4}$  to  $10^{-3}$  Scm<sup>-1</sup> measured on pure TiO<sub>2</sub> membranes made by sol-gel methods was also reported by Tsuru et al.<sup>71</sup> Titania nanotubes functionalized by 3-mercaptopropyltri-methoxysilane (MPTMS) as the sulfonic acid functional group precursor showed a proton conductivity of 0.08 Scm<sup>-1</sup> at 80°C and 100% RH and has been shown to be a good additive to enhance the proton conductivity of Nafion membranes at elevated temperature and reduced RH.<sup>72</sup>

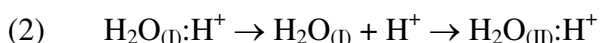
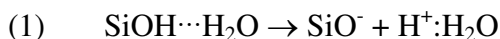
### 3.2. Silica and silica based glass

The ordered nanoporous or mesoporous silica materials with high structural order, large surface areas and pore volumes, and easy and variable surface functionalization offer great potential as porous frameworks not only for catalyst supports, protein separation, CO<sub>2</sub> capture<sup>73,74</sup> but also for catalysts support and proton conductor as high temperature PEM applications.<sup>62,70,75-84</sup> Ye et al.<sup>85</sup> gave an excellent review on the recent applications of mesoporous materials as electrodes in solar cells, fuel cells and batteries. Due to their high hydrophilicity and capillary condensation effects in the nano-channels they can store and release water at elevated temperatures, facilitating

water-assisted proton transport at temperatures above 100°C. The first reports on ordered mesoporous materials with well-defined pore sizes appeared in 1992 when researchers at Mobil reported for the first time on the synthesis of the M41S family.<sup>86, 87</sup> These mesoporous silica, synthesized by the self-assembly method using surfactants as a template, has a large surface area and a uniform pore diameter of several nm.<sup>88</sup> The water vapor condenses in pores through capillary force and this occurs at lower water vapor pressures for smaller pores. Thus, a porous structure with a high surface area and small pores is favorable for proton migration. The pore size and pore structure affect the proton conductivity.<sup>75</sup> The proton conductivity has been found to be associated with surface dehydroxylation of porous silica during the heat-treatment. However, high heat-treatment temperature would reduce the hydrophilic nature of the porous silica glass, leading to the reduced conductivity. Li and Kunitake<sup>89</sup> used oxygen plasma technique to remove the surfactant template, obtaining porous silica thin films at reduced temperatures. The IR data showed that the plasma-treated film had a high retention of the silanol group on the pore wall, as compared to the heat-treated samples. The conductivity of plasma-treated porous silica is  $4.8 \times 10^{-4} \text{ Scm}^{-1}$  at 90% RH and 50°C, an order of magnitude higher than that of the heat-treated porous silica under identical conditions.<sup>89</sup> On the other hand, high proton conductivity of  $2.0 \times 10^{-2} \text{ Scm}^{-1}$  at 80°C and 81%RH was reported on mesoporous silica xerogels with average pore size of 3.7 nm.<sup>90</sup> Proton conductivity of mesoporous silica and silica xerogels showed a pronounced dependence on RH.<sup>89, 90</sup>

Nogami et al.<sup>91</sup> studied in details the proton conductivity in porous silica glass with average pore size of ~1.7 nm and reported that 0.1 mm thick porous silica glasses sintered at 400°C exhibited proton conductivity of  $\sim 3 \times 10^{-4} \text{ Scm}^{-1}$  at 30°C under high RH. The activation energy for conduction decreases linearly with increasing logarithm of the product of proton and water

concentration, and the conductivity increases to the water concentration, as shown in **Figure 2**.<sup>91</sup> Data for glasses containing small amount of water were from ref.<sup>92</sup> The results indicate that proton conduction in porous silica glasses involves the protons dissociated from SiOH bonds and subsequently migration or hopping from the initial site to a neighboring site, resulting in the conductivity, as shown below:<sup>91</sup>



where the dotted line represents the hydrogen bonding between the proton and water molecule,  $\text{H}_2\text{O}_{(\text{I})}$  and  $\text{H}_2\text{O}_{(\text{II})}$  are the water molecules that the proton is hopping between. Thus the proton conductivity of porous silica glasses is highly dependent on the water concentration. However, the proton conductivity of pristine mesoporous silica is generally too low (e.g.,  $10^{-6}$  S  $\text{cm}^{-1}$  to  $10^{-4}$  S  $\text{cm}^{-1}$  under 40% to 90% RH<sup>75, 93</sup>) to be applicable as PEM for fuel cells. Incorporation of aluminium in mesoporous silica framework can significantly enhance its proton conductivity,<sup>94</sup> as the incorporation of aluminium increases the Brønsted acid sites, enhancing the proton conductivity.

As the protons are generated through the dissociation of adsorbed and condensed water, water dissociation and thus proton conduction can be enhanced by increasing the acidity of the material surface by introducing acid groups, including phosphoric acids,<sup>95,96</sup> sulfonic acids,<sup>84,97</sup> and  $\text{HNO}_3$ .<sup>63,98</sup> Strong acidity also contributes to retaining water molecules under low water vapor pressure.<sup>63</sup> The acid-functionalized mesoporous silica materials constitute an alternative and promising class of inorganic PEMs for high temperature operations due to their high charge carrier concentration, adjustable acid group density and oxidation resistance. Suzuki et al.<sup>99</sup> examined the proton conductivity of phosphorus incorporated mesoporous silica. Incorporation of phosphorus during

mesoporous silica formation was found to be effective in improving proton conductivity. A sample with a low P/Si atomic ratio of 0.07 showed the highest proton conductivity above  $10^{-2}$   $\text{Scm}^{-1}$  at 100 to 120°C under saturated water vapor pressure. Nogami *et al.* showed that incorporation of the P=O bond in the glass structure promotes proton dissociation from hydroxyl groups and thus enhances proton conductivity due to the stronger hydrogen bonds.<sup>100</sup> A porous  $\text{P}_2\text{O}_5\text{-SiO}_2$  glass exhibits a significantly high proton conductivity of  $2 \times 10^{-2}$   $\text{S cm}^{-1}$  at room temperature and the proton conduction was suggested to be related to the proton hopping between hydroxyl groups and water molecules.<sup>100</sup> Although the phosphate unit improves proton conductivity, it becomes detached from silicate network upon immersion in water and the conductivity decreases significantly to values similar to those of pure silica.<sup>101</sup> In the case of silicate and phosphate glasses, the content of protons decreases with an increase in the sintering temperature. Thus it is desirable to prepare glasses with a large number of protons at low temperature, like sol-gel process. The gelation time in conventional sol-gel process can take as long as 1-6 months.<sup>102</sup> However, the sol-gel process can be accelerated by proper water/vapor management.<sup>103</sup> Increasing the density of the surface group by immersing in protonic acids such as  $\text{HNO}_3$  showed marginal improvement in proton conductivity of porous silica.<sup>63, 98</sup>

There are many studies focused on the sulfonic acid functionalization.<sup>84, 104-108</sup> Ioroi *et al.*<sup>109</sup> prepared nanoporous silica glass with 3-mercaptopropyltrimethoxysilane and subsequent oxidation of thiol group to sulfonic acid groups, achieving a proton conductivity of  $1.0 \times 10^{-2}$   $\text{Scm}^{-1}$  at 40°C and 95%RH. However, operation at high temperatures results in the loss of grafted  $\text{HSO}_4$ . Marschall *et al.* synthesized sulfonic acid functionalized MCM-41 by microwave assisted co-condensation method.<sup>106</sup> **Figure 3** shows the proton conductivity of  $\text{SO}_3\text{H-MCM-41}$  synthesized by microwave assisted co-condensation method.<sup>106</sup> Microwave irradiation has the

advantage of oxidation of thiol group and removal of the template within a short time. Pristine mesoporous silica, MCM-41 shows a negligible conductivity of  $\sim 10^{-6} \text{ Scm}^{-1}$ , which is the result of a partial dissociation of water molecules in the presence of silanol group. However,  $\text{SO}_3\text{H-MCM-41}$  composite samples very high proton conductivity at elevated temperatures, achieving  $0.2 \text{ Scm}^{-1}$  at  $140^\circ\text{C}$  and 100% RH (Fig.3a). The proton conductivity of  $\text{SO}_3\text{H-MCM-41}$  also increases significantly with relative humidity. The proton transfer inside the sulfonic group functionalized mesopores is suggested to be the Grotthuss-like mechanism.<sup>106</sup> Nevertheless, no cell performance was presented for the  $\text{SO}_3\text{H-MCM-41}$  materials. It has been reported that mesoporous silica impregnated with 5.0M  $\text{H}_2\text{SO}_4$  shows high conductivities in the order of  $10^{-1} \text{ Scm}^{-1}$  in a temperature range from 40 to  $80^\circ\text{C}$  at 60%RH.<sup>110</sup> However, the conductivity decreases drastically with time due to a rapid loss of the impregnated  $\text{H}_2\text{SO}_4$  acid. Marschall et al.<sup>111</sup> synthesized imidazole functionalized mesoporous MCM-41 silica by immersing treatment and the highest conductivity was  $\sim 10^{-4} \text{ S cm}^{-1}$  at  $140^\circ\text{C}$  and 100% RH. The proton conductivity of sulfonic acid and imidazole functionalized mesoporous silica composites was found to be very sensitive to RH.<sup>97, 111</sup>

Qiao et al studied in details the proton conductivity properties of phosphoric or phosphonic acid functionalized mesoporous-structured silica as potential membranes for fuel cells.<sup>112, 113</sup> Owing to the amphoteric nature of the phosphonic acid, such solids can function as a proton donor (acidic) as well as a proton acceptor (basic) to form dynamic hydrogen bond networks in which protons are transported by breaking and forming of hydrogen bonds. The proton conductivity of phosphonic acid functionalized porous silica nanospheres synthesized by the co-condensation of diethylphosphatoethoxysilane (DPTS) and tetraethoxysilane using cetyltrimethylammonium bromide surfactant as a template, followed by acidification to phosphoric acid in concentrated

HCl, depends strongly on the nominal P/Si ratio, the morphology of the porous silica nanosphere and the RH (**Figure 4**).<sup>112</sup> The proton conductivity increases with the humidity and NP40 with most phosphonic acid shows the highest conductivity,  $3.0 \times 10^{-4} \text{ S cm}^{-1}$  at 20% RH to  $0.015 \text{ S cm}^{-1}$  at 100% RH at 130 °C. The results indicate that high surface area of the porous silica enhances the proton conductivity under low humidity conditions. However, no stability and cell performance were reported for the phosphoric acid functionalized silica nanosphere composites.

Research has shown that replacing pure silica with composite silicate of strong acidity, e.g., the  $\text{Cs}_3(\text{H}_2\text{PO}_4)(\text{HSO}_4)_2\text{-SiO}_2$ ,<sup>114</sup>  $\text{CsH}_2\text{SO}_4\text{-SiO}_2$ ,<sup>115</sup>  $\text{P}_2\text{O}_5\text{-SiO}_2$ ,<sup>103</sup>  $\text{P}_2\text{O}_5\text{-TiO}_2\text{-SiO}_2$ <sup>116</sup> or  $\text{P}_2\text{O}_5\text{-ZrO}_2\text{-SiO}_2$ <sup>117</sup> improves the proton conductivity. Due to the higher hydrophilicity of  $\text{P}_2\text{O}_5$  as compared to  $\text{SiO}_2$ , the incorporation of  $\text{P}_2\text{O}_5$  increases the amount of  $\text{H}_2\text{O}/\text{OH}$  hydrogen bonding. Tung et al.<sup>103</sup> indicated that increasing  $\text{P}_2\text{O}_5$  content leads to the increased functional groups of  $\text{P}=\text{O}$  and  $\text{P-OH}$  on the pore surface and reduces the number of major pore size channels. The best conductivity is  $1.14 \times 10^{-2} \text{ S cm}^{-1}$  at 80°C and 100% RH, obtained on 50 $\text{P}_2\text{O}_5$ -50 $\text{SiO}_2$  glass. Nogami et al.<sup>118-124</sup> incorporated various heteropolyacids into silicaphosphate porous glass and yielded an electrolyte membrane with proton conductivity of  $0.1 \text{ S cm}^{-1}$  at 85 °C and 85% RH. The cell based on phosphomolybdic acid (HPMo) incorporated silicaphosphate glass produced a maximum power density of  $32 \text{ mW cm}^{-2}$  at 29 °C and 30% RH (see **Figure 5**).<sup>124</sup> The characteristics of the polarization curves indicate that the cell performance is mainly dominated by the ohmic polarization losses most likely due to the high resistance of the HPMo/ $\text{ZrO}_2\text{-P}_2\text{O}_5\text{-SiO}_2$  glass composite membrane.

The power densities reported for silica-based glass PEMs is generally low, from 6 to 41.5  $\text{mW cm}^{-2}$  on  $\text{P}_2\text{O}_5\text{-SiO}_2$  and HPW/HPM- $\text{P}_2\text{O}_5\text{-SiO}_2$  membranes<sup>125, 126</sup> to 45  $\text{mW cm}^{-2}$  on surface modified silica glass membranes.<sup>109</sup> Using proton conducting  $\text{H}_3\text{PO}_4$  as binder, the power density

of  $\text{P}_2\text{O}_5\text{-SiO}_2$  glass membrane cell was  $70.3 \text{ mW cm}^{-2}$  at  $80^\circ\text{C}$  and  $75\%\text{RH}$ , which is significantly higher than  $28.3 \text{ mW cm}^{-2}$  on the same membrane but with PTFE as the binder.<sup>127</sup> Nakamoto et al obtained maximum power densities of  $\sim 25 \text{ mWcm}^{-2}$  at  $130^\circ\text{C}$  and  $38 \text{ mWcm}^{-2}$  at  $150^\circ\text{C}$  using phosphosilicate gel/polyimide composite membrane.<sup>128</sup> Most recently, Ishiyama et al reported the development of tungsten phosphate glass as PEM for fuel cells.<sup>129</sup> The proton was injected into sodium conductive oxide glass by electrochemical oxidation of hydrogen at Pd anode and the maximum proton conductivity is  $8 \times 10^{-4} \text{ Scm}^{-1}$  at  $300^\circ\text{C}$ . The maximum power density of a cell based on proton injected tungsten phosphate glass membrane is  $1.3 \text{ mWcm}^{-2}$  at  $300^\circ\text{C}$ . Decreasing the membrane thickness as well as the interface resistance is essential to enhance the cell power output of silica glass based membranes. Di et al.<sup>130</sup> introduced a thin Nafion layer to a phosphosilicate glass membrane and the addition of a thin Nafion layer reduced the glass membrane thickness to  $500 \mu\text{m}$ , achieving a peak power density of  $207 \text{ mWcm}^{-2}$  at  $70^\circ\text{C}$  in  $\text{H}_2/\text{O}_2$ . However, the operation temperature of such MEAs would be limited by the thermal stability of the inserted Nafion layer.

### 3.3. $\text{Al}_2\text{O}_3$ and other ceramic materials

Proton conductivity of porous alumina has also been investigated as potential application as PEM for fuel cells. Shen et al.<sup>131, 132</sup> studied the effect of pore size and salt doping on the proton conductivity of mesoporous alumina. Conductivity of mesoporous alumina increased with the pore size and best results were obtained with a pore diameter of  $10.8 \text{ nm}$ ,  $4.0 \times 10^{-3} \text{ Scm}^{-1}$  at  $30^\circ\text{C}$  and  $90\%\text{RH}$ . Doping with chloride improves the proton conductivity by 3 to 6 times that of pure alumina.  $\text{NH}_3\text{-TPD}$  analysis showed that chlorine displaces some surface OH and increased the acidity of the mesoporous  $\text{Al}_2\text{O}_3$ , leading to the increase of the proton conductivity.<sup>133</sup> Mesoporous acid-free hematite ceramic membranes have also been studied as proton conductors by Colomer *et*

*al.*<sup>134</sup> This  $\alpha$ -Fe<sub>2</sub>O<sub>3</sub> ceramic membrane showed a sigmoidal dependence of the conductivity and the water uptake on the RH at a constant temperature. Further study showed that mesoporous  $\alpha$ -Fe<sub>2</sub>O<sub>3</sub> can also be synthesized from a hydrolytic ferric oxide polymer using a microwave-assisted sol-gel route.<sup>135</sup> Despite the unique acid-free property, the highest conductivity of this  $\alpha$ -Fe<sub>2</sub>O<sub>3</sub> ceramic membrane is  $2.76 \times 10^{-3} \text{ S cm}^{-1}$  at 90 °C and 81%RH<sup>135</sup>. Nd<sub>5</sub>LnWO<sub>12</sub> and Ln<sub>6</sub>WO<sub>12</sub> have been found to have satisfactory proton conductivity at high temperature in hydrogen-containing atmosphere, however the coexisting electronic conductivity impedes the use in fuel cells.<sup>136</sup>

Tsui et al.<sup>137</sup> studied the proton conductivity properties of ceramic membranes derived from ferroxane and alumoxane precursors. The ferroxane derived ceramics, FeOOH fired at 300 °C showed highest proton conductivity from 1.29 to  $2.65 \times 10^{-2} \text{ S cm}^{-1}$  at relative humidities of 33–100% and room temperature. The conductivity of ferroxane is comparable to that of the Nafion<sup>®</sup> membrane with the advantages of lower methanol permeability and less sensitivity to humidity, as shown in **Figure 6**.<sup>138</sup> However, the ferroxane ceramic membranes are very brittle and can be easily broken to very small pieces. This is mainly due to the poor mechanical properties of the precursor, lepidocrocite as compared to other ceramic materials such as silica and alumina. For example, the hardness of lepidocrocite is 5 GPa, significantly lower than 30.6 GPa obtained on silica.<sup>139</sup> This makes it very hard to fabricate membranes from ferroxane-based ceramic powders.

#### 4. Heteropolyacids functionalized mesoporous silica

In recent years, we concentrated our efforts on the development of heteropolyacids (HPAs) -functionalized mesoporous silica as new inorganic high temperature PEM for fuel cells.<sup>28, 140, 141</sup> HPAs are known to be a Brønsted acid with unique nano-sized structures and a very strong acidity. Crystallized HPAs contain two types of protons in their structures: the water-combining proton which is dissociated and hydrated, the other is the unhydrated proton located on the bridge-oxygen



in the HPAs.<sup>142</sup> Among HPAs, phosphotungstic acid ( $\text{H}_3\text{PW}_{12}\text{O}_{40}$ , abbreviated as HPW) has the highest stability and strongest acidity with a high proton conductivity in fully hydrated state,  $0.18 \text{ S cm}^{-1}$ .<sup>143</sup> The most common structure is Keggin Unit (KU) as shown in **Figure 7**. The central phosphorus (P) atom in a tetrahedral environment is surrounded by 12 octahedral of composition  $\text{WO}_6$ . The oxygen atoms are shared by tungsten atoms, except for 12 terminal oxygen atoms ( $\text{O}_t$ ) attached to only one addenda atom (W). Normally, protons coordinate to oxygen atoms on the exterior of the KU to construct the primary structure of the HPA. Then adsorbed water molecules interact with oxygen atoms of adjacent KUs via hydrogen bonds, linking the units together to form a secondary structure. The effect of water on proton conductivity of HPW is well known, which is pertinent to the use of HPW in the PEM fuel cells.<sup>144-147</sup> Another reason for the selection of HPW as proton carrier in the *meso*-silica matrix is the high thermal stability, upto  $500 \text{ }^\circ\text{C}$ .<sup>148</sup>

#### ***4.1 Synthesis of HPW functionalized mesoporous silica nanocomposites***

There are two main approaches to anchor the acid or organic groups onto the inner pore surface of the mesoporous silica: the grafting/impregnation method (post synthesis) and the co-condensation method (direct or one-pot synthesis). For example, grafting of an organotrialkoxysilane  $\text{RSi}(\text{OR}')_3$  onto the inner surface of the mesoporous silica is well established.<sup>149, 150</sup> This method is generic and allows for the incorporation of many different acids and R groups, including bulky ones. The disadvantage of the post synthesis method is that neither the loading nor the surface distribution of the function groups as well as their accessibility can be easily controlled. On the other hand, a one-pot synthesis method has the advantages of precise control of the density and distribution of the function groups along the pores.<sup>106, 151, 152</sup> Marschall et al. showed that the loading of sulfonic acid group,  $-\text{SO}_3\text{H}$  of the samples synthesized by the co-condensation method is much higher compared to that functionalized by grafting method.<sup>106, 107</sup>

Bibent et al synthesized mesoporous SBA-15 with phosphonic, sulfonic and carboxylic acid functional groups by a one-pot synthesis method, see **Figure 8**.<sup>153</sup> The acid functionalized mesoporous silica were prepared by co-condensation of the Pluronic 123 (P123, poly(ethylene oxide)-poly(propylene oxide)-poly(ethylene oxide) (PEO-PPO-PEO) block copolymer commercially available as amphiphilic polymers) with a mixture of  $[(\text{EtO})_3\text{Si}(\text{CH}_2)_3\text{-X}]$  and tetraethoxysilane (TEOS), where  $\text{X} = \text{PO}(\text{OEt})_2$ , SH or CN. The results indicate that the proton conductivity is directly related to the acidity and density of the functional groups anchored to the mesopore surface.

HPW can be incorporated into the mesoporous silica matrix by post synthesis or by one-pot self-assembly synthesis process.<sup>28, 140</sup> HPW is soluble in water, forming negatively charged  $\text{PW}_{12}\text{O}_{40}^{3-}$  ions. Under normal conditions, the proton adsorption on the SiOH surface groups of the *meso*-silica is very low. However, the presence of HPW decreases the pH of the precursor as HPW is highly acidic in water and this in turn significantly increases the proton adsorption of SiOH groups, forming positively charged  $\text{SiOH}_2^{+1}$ .<sup>154</sup> When HPW molecules, silica precursor, TEOS are mixed in water, self-assembly occurs between the positively charged silica and the negatively charged HPW by the electrostatic force. With the addition of structure-directing agent, P123, the tube-cumulated mesoporous HPW-silica with the template of P123 surfactant is formed through the cooperative hydrogen bonding and self-assembly between the HPW-silica structure and P123 surfactant.<sup>88</sup> With the phase separation of P123, the colloidal complex forms ordered mesoporous silica with the HPW self-assembled in the mesoporous structure. The surfactant template is then removed by the heat treatment at 400°C. In the case of post synthesis method, HPW is impregnated into mesopores of mesoporous silica synthesized by methods reported in the literature,<sup>88</sup> followed

by solution impregnation preferably under vacuum.<sup>28</sup> **Figure 9** shows the principles of the two synthesis approaches.<sup>148, 155</sup>

The HPW loading in the mesoporous silica matrix depends on the synthesis method. In the case of impregnation route, the HPW loading can be as high as 80 wt%, while the maximum HPW content which can be incorporated into *meso*-silica structure without significant detrimental effect on the mesoporous structure is ~25 wt% in the case of one-pot synthesis route.

## 4.2 Microstructure, conductivity and performance

### 4.2.1 Microstructure

The microstructure of HPW functionalized mesoporous silica, HPW-*meso*-silica is related to the synthesis methods. In the case of HPW-*meso*-silica synthesized by two-step post synthesis method, the distribution of HPW inside the mesopores can be directly identified by TEM (see **Figure 10**).<sup>148</sup> The mesoporous silica host was characterized by highly ordered nano-channels and the channel diameter of mesoporous silica is ~5.2 nm as shown in Figure 10a. In the case of HPW-*meso*-silica nanocomposites, the distribution of the impregnated HPW nanoparticles in the mesoporous silica matrix is indicated by the ordered but not continuous black dots sandwiched between continuous channels (grey in color, see Figure 10b and 10c). The thick line structure in grey color is siliceous pore walls and the phase contrast between HPW and silica becomes pronounced as the HPW content in the nanocomposite increased to 80wt% (see the inset, Fig.10c). Such phase contrast was also observed in the cesium substituted HPA-*meso*-silica system.<sup>156</sup> As the HPW content in *meso*-silica increased to 80 wt%, the density of HPW particles increases, indicating the distribution of HPW particles in 80%HPW-*meso*-silica is much more uniform than that of 20%HPW-*meso*-silica. The higher intensity of HPW particles inside the *meso*-silica means shorter pathway of proton transportation, which would lead to the high proton conductivity and

low activation energy barriers for the proton conductance in the *meso*-silica matrix. The average distances between the HPW particles in the HPW-*meso*-silica nanocomposites vary between 0 to 5 nm, and the shape and diameter of the interconnected channels of HPW-*meso*-silica nanocomposites are not as regular as that of the pristine *meso*-silica host (the inset, Fig.10c), probably due to the impregnation and insertion of HPW particles.

The post synthesis method also has advantages in the flexibility of easy control of mesoporous silica structure symmetries. The pore size and volume can be monitored by variation of the post synthesis hydrothermal treatment conditions.<sup>157</sup> We investigated recently HPW-*meso*-silica membrane with mesoporous silica from 2D hexagonal  $p6mm$ , 3D face-centered cubic ( $Fm\bar{3}m$ ), body-centered  $Im\bar{3}m$ , to cubic bicontinuous  $la\bar{3}d$  symmetries.<sup>158</sup> HPW-*meso*-silica nanocomposites with 3D mesostructures display a significantly higher proton conductivity and higher stability as a function of relative humidity in comparison to 2D mesostructures.

The formation and size of micelle and consequently the structure and size of mesopores of mesoporous silica by one-pot synthesis method are highly dependent on the size of the function group. This is indicated by the limit of the HPW loading which can be added to the synthesis solution in order to have high density of HPW and at the same time to maintain the high degree of the mesoporous order of the functionalized mesoporous silica.<sup>140, 155</sup> **Figure 11** is the TEM micrographs of the ordered mesoporous structure of *meso*-silica with different HPW contents, synthesized via one-pot self-assembly route.<sup>155</sup> The as-synthesized HPW-*meso*-silica structure is characterized by highly ordered 2D nanochannels. The center to center distance of the nanochannels is  $\sim 7.3$  nm (Fig.11a). From the TEM images viewing along the pore axis, the diameter of the hexagonal mesostructure is 4.3 nm for 5wt% HPW-*meso*-silica (Fig.11b) and 3.8 nm for 25wt% HPW-*meso*-silica (Fig.11c). The high-resolution TEM micrograph unambiguously

demonstrates that the hexagonal packing of the nanochannels is well-aligned along the zone axis [001] direction. The uniformly ordered mesoporous arrays are still maintained when the HPW content is less than 25wt%. The top-surface feature is reflective of long-range ordering of the mesochannels and their macroscopic alignment.<sup>159</sup> The results indicate the successful assembly of HPW molecules into the mesoporous SBA-15 structure. However, for the 35wt% self-assembled HPW-*meso*-silica, the mesostructure becomes discontinuous and distorted (see Figure 11d). The collapse of the ordered mesoporous structure is consistent with the observed significant shrinkage of the diffraction peak (100) of SAXS.<sup>155</sup>

#### 4.2.2 Conductivity and cell performance

Similar to the sulfonic acid functionalized mesoporous silica materials, the proton conductivity of HPW-*meso*-silica nanocomposites depends strongly on the HPW content. In the case of HPW-*meso*-silica nanocomposites via impregnation route, the threshold of HPW content is ~10 wt%. When the HPW content reaches 65-67 wt%, the conductivity is almost independent of the HPW content and remains a constant value of 0.07 S cm<sup>-1</sup> at 25°C and 100% RH, see **Figure 12**.<sup>148</sup> Similar trend was also observed on one-pot self-assembled HPW-*meso*-silica nanocomposites with the maximum conductivity on 25 wt% HPW-*meso*-silica.<sup>155</sup> The proton conductivity is also affected by the structure of the mesoporous silica matrix.<sup>158</sup> The best result was obtained with body-centered cubic ( $Im\bar{3}m$ )-HPW-*meso*-silica, showing proton conductivities of 0.061 S cm<sup>-1</sup> at 25 °C and 0.14 S cm<sup>-1</sup> at 150 °C under 100% RH, respectively and an activation energy of 10.0 kJ mol<sup>-1</sup>. Most importantly, the proton conductivity of HPW-*meso*-silica has a much lower sensitivity toward the change in relative humidity. **Figure 13** shows the dependence of the conductivity of a HPW-*meso*-silica nanocomposite on RH measured at 80°C.<sup>157</sup> In the figure, the proton conductivity of Nafion 115 membrane was measured at 30°C as a function of RH. The initial rapid

rise in conductivity originates from a change in the hydration state of HPW as the conductivity of HPW is strongly dependent on the number of water molecules contained in the HPW KU (noted as  $\text{H}_3\text{PW}_{12}\text{O}_{40}\cdot n\text{H}_2\text{O}$ ,  $n=4\sim 29$ ). However, the RH dependence of the conductivity is far less sensitive as compared to that of Nafion membranes.<sup>160, 161</sup> The much less sensitivity of the proton conductivity on the RH indicates the high water retention of the HPW KU-type nanoparticles anchored in the ordered meso-silica structure.

Leaching of acid function groups from functionalized mesoporous silica is a very important issue for the practical application of the materials as PEMs for fuel cells. The stability of the anchored HPW inside the mesopores was assessed by measuring the stability of proton conductivity of HPW-*meso*-silica under an accelerated durability test with a constant water flow. In the case of a 80%HPW-*meso*-silica, the conductivity value of the nanocomposites drops rather rapidly during the first few hours and reaches a constant value after tested for 6 h under an accelerated durability test at 80 °C with a constant water flow rate.<sup>28</sup> For example, the conductivity decreased from 0.108 and to stabilized at 0.075 S cm<sup>-1</sup> after 6h test and the loss in proton conductivity is 28%.<sup>28</sup> The initial decay in the conductivity is most likely due to the leaching of HPW during the flushing of water. The stability of the impregnated HPW also depends on the pore size. The mesoporous silica with pore size of ~5 nm shows a much higher retention ability for impregnated HPW as compared to that with larger pore size.<sup>157</sup> The stabilized conductivity indicates the successful immobilization of water soluble HPW in the mesoporous silica framework. On the other hand, the HPW-*meso*-silica synthesized by one-pot synthesis method shows a very stable proton conductivity under elevated temperature and reduced RH.<sup>155, 162</sup> The stability of HPW inside the mesoporous silica is most likely due to the formation of  $(\equiv\text{SiOH}_2^+)(\text{H}_2\text{PW}_{12}\text{O}_{40}^-)$  species.<sup>162, 163</sup>

The applicability of HPW-*meso*-silica nanocomposite PEMs has been demonstrated in both H<sub>2</sub> and alcohol fuels such as methanol and ethanol on small button cells.<sup>28, 155, 158, 162</sup> **Figure 14** is the typical cell performance for direct methanol and ethanol fuel measured at different temperatures on a cell with a 165  $\mu\text{m}$ -thick 25wt% HPW-*meso*-silica nanocomposite membrane synthesized via one-pot synthesis method and conventional Pt-based electrocatalysts.<sup>162</sup> The open circuit potential is low, 0.6-0.65V probably due to the electrolyte membrane which is not 100% dense. The maximum power density is 16.8 and 43.4  $\text{mW cm}^{-2}$  for direct ethanol and methanol at 80°C, respectively, indicating low electrocatalytic activity of Pt electrocatalysts for the electrochemical oxidation reactions of ethanol and methanol at low temperatures. As the temperature is raised to 200°C, the maximum power output is 112  $\text{mW cm}^{-2}$  for direct ethanol fuel cell and 128.5  $\text{mW cm}^{-2}$  for direct methanol fuel cell. The DMFC performance based on HPW-*meso*-silica nanocomposite membrane and low Pt catalyst loading (1  $\text{mg cm}^{-2}$ ) is close to the advanced DMFCs (100-200  $\text{mW cm}^{-2}$ ).<sup>164</sup> The preliminary cell stability was tested under a constant current density of 300  $\text{mA cm}^{-2}$  at 200°C for ~ 1 h. The cell performance indicates the elimination of poisoning effect of the alcohol oxidation reaction on the Pt black catalysts at elevated high temperatures (Fig.14b), very different from that commonly observed significant drop in performance for the DAFCs at low temperatures.<sup>165</sup> Further study showed that maximum power density of the cell can be as high as ~240  $\text{mWcm}^{-2}$  at 150°C in 10%RH or under no external humidification in methanol fuel.<sup>155, 158</sup> The studies also show that HPW-*meso*-silica nanocomposites have a much lower methanol crossover as compared to the Nafion membranes, most likely due to the gas phase diffusion of methanol and dimensional stability of the inorganic nanocomposite.

Demonstration of the performance in stack cells rather than small button cells is an essential step towards the practical application of inorganic PEMs like HPW-*meso*-silica. However, very

different from polymeric membrane such as Nafion and PBI/PA membranes,<sup>166-170</sup> the fabrication of homogeneous, crack-free and mechanically strong membranes with a good working surface area is a significant technological challenge for acid functionalized inorganic materials. Most recently, we successfully fabricated relatively large HPW-*meso*-silica nanocomposite membranes and demonstrated the good performance of the membranes in PEM fuel cell stacks in H<sub>2</sub> without external humidification.<sup>171</sup> HPW-*meso*-silica nanocomposite membranes were fabricated by a modified hot-pressing process so as to increase the mechanical strength and increase the size of membrane. **Figure 15** shows the power output of the 10-cell stack assembled with a 0.76 mm-thick HPW-*meso*-silica membrane and Pt/C as both catalyst anode and cathode in H<sub>2</sub>/O<sub>2</sub>.<sup>171</sup> The OCV of the stack is 7.9 V. The stack produced a maximum power output of 74.4 W, corresponding to a power density of 372.1 mW cm<sup>-2</sup> at 150 °C in H<sub>2</sub>/O<sub>2</sub> based on the total effective cell area of 200 cm<sup>2</sup>. This power output is quite high compared to values reported on alternate inorganic membrane fuel cells such as In<sup>3+</sup> doped SnP<sub>2</sub>O<sub>7</sub> (264 mW cm<sup>-2</sup> at 250 °C),<sup>172</sup> CsH<sub>2</sub>PO<sub>4</sub>-based electrolyte (48.9 mW cm<sup>-2</sup> at 235 °C),<sup>173</sup> and HPMo/HPW doped glass electrolytes (32 mW cm<sup>-2</sup> at 29 °C).<sup>124</sup> The 10-cell stack demonstrates high stability during a 50 h test and generated a near-constant power output of ~32 W in H<sub>2</sub>/air (viz., power density of 160 mW cm<sup>-2</sup>) at 150 °C without external humidification (see Fig.15b). The results indicate that the HPW-*meso*-silica nanocomposites can be applied in PEM fuel cell stacks operated at elevated temperature in the absence of external humidification.

#### 4.3 Proton hopping within HPW-*meso*-silica nanocomposite

Within HPW-*meso*-silica membrane, the negative charged heteropolyacid PW<sub>12</sub>O<sub>40</sub><sup>3-</sup> are anchored inside the mesoporous silica channels most likely due to the formation of (≡SiOH<sub>2</sub><sup>+</sup>)(H<sub>2</sub>PW<sub>12</sub>O<sub>40</sub><sup>-</sup>) species.<sup>162</sup> As shown in Figure 10, TEM has provided a direct



observation of the morphology and distribution of HPW nanoparticles in the highly ordered mesoporous silica channels, in which the distances between HPW vary according to the weight percentage of HPW. When the content of HPW increases, the average distance between HPWs is accordingly decreased, which leads to the decrease of the energy barrier of proton transfer, so does the increase of the proton conductivity (see Fig.12).<sup>148, 157</sup> For pristine mesoporous silica, the activation energy for proton transfer is 47-55 kJ mol<sup>-1</sup> and it is 10-14 kJ mol<sup>-1</sup> for the proton conductivity on HPW-*meso*-silica.<sup>140, 148, 158</sup> Clearly, the average distances between HPWs, determined by the HPW loading, affect both the proton conductivity and energy barrier of proton transfer. **Figure 16** depicts the effective proton transport pathways in the HPW functionalized mesoporous silica. There are two effective pathways determining the rate of proton transfer. One is the intramolecular proton transfer pathway, in which the proton-hopping happens on an isolated HPW. The other is the intermolecular proton transfer pathway, which differs from the intra-pathway since the proton-exchange process is composed of a series of “hops” from one HPW to the neighboring HPW along the water-assisted hydrogen bond. Obviously, the pathway with higher energy barrier will be the rate-limited step, and determines the overall proton conductivity of HPW-*meso*-silica nanocomposite.

## 5. Prospect of functionalized mesoporous silica for high temperature PEMFCs

Table 1 summarizes the properties and performance of typical functionalized mesoporous inorganic materials based PEMs. As shown in Table 1, doping of proton conducting agents such as phosphate and sulfuric acids are effective to enhance the proton conductivity of the mesoporous materials. The highest power out was observed on the cell with PA functionalized sintered meso-silica membranes, 570 mW cm<sup>-2</sup> at 190°C in H<sub>2</sub>/O<sub>2</sub>.<sup>174, 175</sup>

However, for a PEMFC with capability to operate at high temperatures in the range of 200-450°C it essentially requires a PEM with adequate proton conductivity and stability. To achieve high proton conductivity, the functionalized mesoporous materials must have the capability to retain or hold water under conditions of high temperatures and low RH. As the temperature increases, the total pressure required to maintain the same RH increases dramatically. For example, as shown by Zhang et al.<sup>16</sup> to maintain 100% RH at 180°C requires a total pressure of >10 atm even without considering the partial pressure of fuel and oxidant gas. This essentially places a requirement of the adequate proton conductivity of the functionalized mesoporous materials under very low RH at high temperatures in order to achieve adequate power output under normal operation (i.e., low pressure) conditions. The degree of structural order and size of the mesopores of the porous matrix as well as the structure of the anchored proton carrier have considerable effect on the water retention properties of the system. On the other hand, the durability of PEMs depends largely on the stability of proton carriers within the mesopores of the matrix, which in turn is related to the nature of the interaction between the dopant and host mesoporous materials. If no chemical bonds are formed between the proton carrier and the exterior surface of mesoporous matrix, there might be considerable effect of leaching out proton carrier due to water produced in a running fuel cell.

Mesoporous materials without doping of proton carrier generally show significant dependence on the RH. For example, for mesoporous zirconium phosphates,  $\sigma$  is  $4.1 \times 10^{-6}$  at 22°C and 84% RH and when RH decreases to 30%,  $\sigma$  is  $\sim 3.0 \times 10^{-8}$  at the same temperature,<sup>37</sup> resulted in a conductivity decrease by more than two orders of magnitude. Thus, the nature of the proton carrier or conductor is critical. For example, phosphates are lacking in chemical stability as  $P^{5+}$  ions are easily dissolved in water and becomes detached from the silicate network.<sup>101</sup> Rapid

decrease in conductivity was also observed on sulfuric acid impregnated mesoporous silica glass membrane due to a partial or total loss of the impregnated acid.<sup>106</sup> Membranes based on phosphate-silicate glasses show the performance at temperature as high as 300°C, but the conductivity and cell performance ( $\sigma = 8 \times 10^{-4} \text{ Scm}^{-1}$  and  $P = 1.3 \text{ mWcm}^{-2}$  at 300°C)<sup>129</sup> are probably too low for practical applications. The proton conductivity of phosphate functionalized mesoporous silica also shows high sensitivity to humidity.<sup>112</sup> One of the most fundamental reasons for the leaching of proton carriers such as phosphate and sulfuric acid is most likely the lack of strong chemical bonding between the proton carriers and the  $\text{ZrO}_2$ ,  $\text{TiO}_2$  and  $\text{SiO}_2$  based mesoporous matrix.

Mesoporous structures that possess ordered and interconnected networks and high surface areas have shown advantages as support matrix for proton carrier when used as PEMs of fuel cells. However, the control of crystallinity, pore size, porosity and ordering in the mesoporous materials is critical to obtain optimum performance as supports for proton carrier. For example, HPW-*meso*-silica nanocomposites with 3D mesostructures display a significantly higher proton conductivity and higher stability as a function of relative humidity in comparison to 2D mesostructures.<sup>158</sup> For unsupported mesoporous materials, e.g.,  $\alpha\text{-Fe}_2\text{O}_3$  and  $\text{P}_2\text{O}_5\text{-SiO}_2$  glass, high specific surface areas, high pore volume and narrow pore size distribution in the range of 2-3 nm would be required to maintain high water uptake and thus adequate conductivity.<sup>91, 127, 135</sup> In this case, water molecules within the mesopores play a major role in proton transport by forming protonic charge carriers through hydrogen bonding. On the other hand, size of nano or mesopores is related to the proton carrier or dopant. In the case of HPW as proton carrier, pore size in the range of ~6 nm would be sufficient to maintain high proton conductivity and stability.<sup>157</sup> Large pores will lead the significant loss of the impregnated HPW from the HPW-*meso*-silica

nanocomposites. Thermal stability and sintering ability of the mesoporous structure is also important parameter if the fabrication of the mesoporous materials based membrane involves the high temperature sintering process. For example, mesoporous structure of  $\text{TiO}_2$  is thermally stability at  $450^\circ\text{C}$ ,<sup>61</sup> but sintering ability of  $\text{TiO}_2$  at this temperature is not known.

As shown here, functionalized mesoporous silica materials show the most promising properties as alternative PEMs for high temperature operation. The proton conductivity of the acid functionalized mesoporous silica is comparable with that of Nafion membranes and under conditions of high temperature and reduced humidity, it is significantly better than Nafion membranes.<sup>84, 106, 140, 148</sup> Among acid functionalized mesoporous silica materials, HPAs such as HPW functionalized mesoporous silica, HPW-*meso*-silica appears to be most promising, achieving a proton conductivity of  $0.14 \text{ S cm}^{-1}$  under  $150^\circ\text{C}$  and anhydrous conditions.<sup>158</sup> The most significant aspect of the HPW-*meso*-silica nanocomposites is the formation of  $(\equiv\text{SiOH}_2^+)(\text{H}_2\text{PW}_{12}\text{O}_{40}^-)$  species between the positively charged siliceous surface of mesoporous silica and negatively charge HPW in the presence of water.<sup>162</sup> This ensures the immobilization and high stability of impregnated or assembled HPW within a highly ordered mesoporous silica structure. The good performance and preliminary stability data of the small button cells and stacks with HPW-*meso*-silica nanocomposite membranes demonstrate that the inorganic PEMs based on highly ordered HPW-*meso*-silica nanocomposites can be applied to fuel cell operated at temperatures up to  $200^\circ\text{C}$ .

However, silica based materials are inherently inflexible and brittle. Thus it is difficult to fabricated MEAs with good interface contact between the electrode and electrolyte under pressurized conditions similar to that of the polymeric materials based membranes. Mechanical strength of silica based membrane is also a problem and it is very difficult to fabricate MEAs with

high density and adequate mechanical strength for handling and operation. Tezuka et al used glass paper as support of a hybrid gel membranes made from 3-glycidoxypropyltrimethoxysilane (GPTMS), tetramethoxysilane (TMOS) and orthophosphoric acid, achieving a power density of  $85 \text{ mWcm}^{-2}$  at  $130^\circ\text{C}$  and 7% RH.<sup>176</sup> The utilization of glass paper reduces the thickness of the hybrid gel membranes. It is also possible to use thin film technique to reduce the thickness of the inorganic materials based membranes. Li et al deposited proton conducting thin films of hafnium phosphate and zirconium phosphate/borate/sulfate on smooth ITO glass substrate with thickness of 100-350 nm.<sup>177</sup> However, in practice the quality of the thin film is critically dependent on the morphology and porous structure of the substrates, which also needs to be catalytically active and electronic conducting as electrodes for fuel cells.

As the ceramic materials are generally in powdered form and thus the membranes fabricated by conventional die pressing techniques need to be in the thickness range of 0.5 to 1.0 mm in order to have sufficient mechanical strength. Nakamoto et al used carbon paper to sandwich phosphosilicate gel and reduced the thickness of the membrane to  $\sim 100\mu\text{m}$  after hot-press at  $130^\circ\text{C}$  under 11 MPa.<sup>128</sup> However, the use of carbon paper and polyimide binder limits the thermal stability of the membrane at high temperatures. Thick membrane results in high ohmic losses in the PEMFC. Furthermore, the mechanical strength of the die-pressed discs is still low and brittle in nature, making it very difficult to scale up the system to fuel cell stacks. Very different from the polymeric materials, such difficulty appears to be one of the major obstacles in the development of inorganic materials based PEM fuel cells. Another issue is the testing a PEMFC at high temperatures as the temperature increases, the total pressure required to maintain the same RH increases dramatically. This essentially places a requirement of the adequate proton conductivity of the inorganic materials under very low RH at high temperatures in order to utilize the

conventional fuel cell test stations. The technical hurdles appear to be indirectly indicated by the observations that majority of open literatures report the excellent proton conductivity of acid functionalized nano or mesoporous ceramic materials such as mesoporous TiO<sub>2</sub>, FeOOH, silica or P<sub>2</sub>O<sub>5</sub>-SiO<sub>2</sub> glass materials but with little or no cell performance.<sup>63, 84, 91, 94, 103, 106, 108, 135, 153, 178, 179</sup> Additionally, the use of polymeric binders in the die-pressed discs also limits operation temperatures (200°C or below) of the PEM due to degradation and decomposition of the polymeric binder.

One of the solutions to substantially increase the operation temperature as well as the mechanical strength is to get rid of polymeric binder. We have found out recently that mesoporous silica powder can form dense membranes after sintering at 650°C with ordered mesoporous structure still intact.<sup>174</sup> The mechanical strength of sintered *meso*-silica is 51 MPa, significantly higher than ~5 MPa on hot-pressed *meso*-silica membranes.<sup>162</sup> The feasibility of utilization of sintered *meso*-silica based PEMs has been demonstrated by functionalization of the sintered *meso*-silica with phosphoric acid (PA) and the results indicate that the PA/sintered *meso*-silica PEMs exhibits excellent conductivity under non-humidified conditions, producing a maximum power density of 689 mW cm<sup>-2</sup> in H<sub>2</sub> at 190°C in the absence of external humidification.<sup>174</sup>

The mesoporous structure of the sintered *meso*-silica is thermally stable at temperatures up to 650°C.<sup>175</sup> If HPW instead of PA is used to functionalize sintered mesoporous silica, the HPW/sintered *meso*-silica nanocomposite could be used for PEMFCs operating at temperatures as high as 450°C, noting that HPW is thermally stable up to 500°C.<sup>148</sup> Preliminary results indicate the open circuit potential of ~0.85 V and power output of ~8 mWcm<sup>-2</sup> at 450°C in H<sub>2</sub>/air using HPW/sintered *meso*-silica nanocomposite PEMs and Ni anode and Pt cathode (see **Figure 17**). The viability of the operation of PEMFCs in the temperature range of 300-450°C fills an important

temperature gap in current fuel cell technologies and demonstrates the promising potentials in the development of new types of fuel cells based on liquid fuels such as methanol and ethanol.

From a practical point of view, power output of  $\sim 8 \text{ mWcm}^{-2}$  would be too low. Thus to substantially increase the cell performance of such functionalized sintered meso-silica nanocomposite based PEMFCs, it is necessarily to develop and optimize new classes of electrocatalysts for the catalysts/meso-silica electrolyte interface. Conventional high surface area carbon-supported Pt based electrocatalysts developed for low temperature fuel cells would not be applicable due to the significant agglomeration of nano-sized Pt catalysts at such high temperatures and oxidation of carbon based supports. However, high operation temperatures in the range of 300-450°C opens a window for the development of non-precious metal and metal oxides based electrocatalysts for fuel cells. Nano-scale and nano-structured electrode concept developed for high temperature solid oxide fuel cells may be applicable for the operation of a PEM fuel cell in the temperatures of 300 to 450°C.<sup>180</sup> In the meantime, considerable more efforts should be made to fundamentally understand the mesoporous structure-property relationships and mechanism and kinetics of the interfacial reactions and phenomena of fuel cells at temperatures up to 450°C.

### Acknowledgement

The work has been supported by the Australian Research Council (DP120102325). I would like to thank Dr Zhou Yuhua for the assistance in providing the graphics in Figure 7 and Figure 16.

### References:

- 1 P. Costamagna, S. Srinivasan, *Journal of Power Sources*, 2001, **102**, 242-252.
- 2 P. Costamagna, S. Srinivasan, *Journal of Power Sources*, 2001, **102**, 253-269.

- 3 F. de Bruijn, *Green Chemistry*, 2005, **7**, 132-150.
- 4 S. Gamburzev, A. J. Appleby, *Journal of Power Sources*, 2002, **107**, 5-12.
- 5 D. E. Curtin, R. D. Lousenberg, T. J. Henry, P. C. Tangeman, M. E. Tisack, *Journal of Power Sources*, 2004, **131**, 41-48.
- 6 A. Brouzgou, A. Podias, P. Tsiakaras, *Journal of Applied Electrochemistry*, 2013, **43**, 119-136.
- 7 K. A. Mauritz, R. B. Moore, *Chemical Reviews*, 2004, **104**, 4535-4585.
- 8 K. D. Kreuer, *Journal of Membrane Science*, 2001, **185**, 29-39.
- 9 C. Yang, S. Srinivasan, A. B. Bocarsly, S. Tulyani, J. B. Benziger, *Journal of Membrane Science*, 2004, **237**, 145-161.
- 10 Y. Sone, P. Ekdunge, D. Simonsson, *Journal of the Electrochemical Society*, 1996, **143**, 1254-1259.
- 11 A. V. Anantaraman, C. L. Gardner, *Journal of Electroanalytical Chemistry*, 1996, **414**, 115-120.
- 12 W. H. J. Hogarth, J. C. D. da Costa, G. Q. Lu, *Journal of Power Sources*, 2005, **142**, 223-237.
- 13 M. Casciola, G. Alberti, M. Sganappa, R. Narducci, *Journal of Power Sources*, 2006, **162**, 141-145.
- 14 Q. F. Li, R. H. He, J. A. Gao, J. O. Jensen, N. J. Bjerrum, *Journal of the Electrochemical Society*, 2003, **150**, A1599-A1605.
- 15 Q. F. Li, R. H. He, J. O. Jensen, N. J. Bjerrum, *Chemistry of Materials*, 2003, **15**, 4896-4915.
- 16 J. L. Zhang, Z. Xie, J. J. Zhang, Y. H. Tanga, C. J. Song, T. Navessin, Z. Q. Shi, D. T. Song, H. J. Wang, D. P. Wilkinson, Z. S. Liu, S. Holdcroft, *Journal of Power Sources*, 2006, **160**, 872-891.
- 17 N. L. Garland, J. P. Kopasz, *Journal of Power Sources*, 2007, **172**, 94-99.
- 18 M. Doyle, S. K. Choi, G. Proulx, *Journal of the Electrochemical Society*, 2000, **147**, 34-37.
- 19 H. W. Zhang, P. K. Shen, *Chemical Society Reviews*, 2012, **41**, 2382-2394.
- 20 A. Iulianelli, A. Basile, *International Journal of Hydrogen Energy*, 2012, **37**, 15241-15255.
- 21 C. Yang, P. Costamagna, S. Srinivasan, J. Benziger, A. B. Bocarsly, *Journal of Power Sources*, 2001, **103**, 1-9.
- 22 H. Ahmad, S. K. Kamarudin, U. A. Hasran, W. R. W. Daud, *International Journal of Hydrogen Energy*, 2010, **35**, 2160-2175.
- 23 V. Neburchilov, J. Martin, H. J. Wang, J. J. Zhang, *Journal of Power Sources*, 2007, **169**, 221-238.
- 24 O. Paschos, J. Kunze, U. Stimming, F. Maglia, *Journal of Physics-Condensed Matter*, 2011, **23**.
- 25 S. M. Haile, D. A. Boysen, C. R. I. Chisholm, R. B. Merle, *Nature*, 2001, **410**, 910-913.
- 26 P. Heo, M. Nagao, M. Sano, T. Hibino, *Journal of the Electrochemical Society*, 2008, **155**, B92-B95.
- 27 Y. Huang, Q. F. Li, A. H. Jensen, M. Yin, J. O. Jensen, E. Christensen, C. Pan, N. J. Bjerrum, W. Xing, *Journal of Materials Chemistry*, 2012, **22**, 22452-22458.
- 28 S. F. Lu, D. L. Wang, S. P. Jiang, Y. Xiang, J. L. Lu, J. Zeng, *Advanced Materials*, 2010, **22**, 971-976.
- 29 K. T. Adjemian, S. J. Lee, S. Srinivasan, J. Benziger, A. B. Bocarsly, *Journal of the*



- Electrochemical Society*, 2002, **149**, A256-A261.
- 30 R. Zeng, Y. Wang, S. L. Wang, P. K. Shen, *Electrochimica Acta*, 2007, **52**, 3895-3900.
- 31 B. P. Ladewig, R. B. Knott, A. J. Hill, J. D. Riches, J. W. White, D. J. Martin, J. C. D. da Costa, G. Q. Lu, *Chemistry of Materials*, 2007, **19**, 2372-2381.
- 32 S. P. Nunes, B. Ruffmann, E. Rikowski, S. Vetter, K. Richau, *Journal of Membrane Science*, 2002, **203**, 215-225.
- 33 F. Pereira, K. Valle, P. Belleville, A. Morin, S. Lambert, C. Sanchez, *Chemistry of Materials*, 2008, **20**, 1710-1718.
- 34 Y. S. Kim, F. Wang, M. Hickner, T. A. Zawodzinski, J. E. McGrath, *Journal of Membrane Science*, 2003, **212**, 263-282.
- 35 B. Tazi, O. Savadogo, *Electrochimica Acta*, 2000, **45**, 4329-4339.
- 36 L. Wang, B. L. Yi, H. M. Zhang, D. M. Xing, *Electrochimica Acta*, 2007, **52**, 5479-5483.
- 37 W. H. J. Hogarth, J. C. D. da Costa, J. Drennan, G. Q. Lu, *Journal of Materials Chemistry*, 2005, **15**, 754-758.
- 38 J. H. Won, H. J. Lee, K. S. Yoon, Y. T. Hong, S. Y. Lee, *International Journal of Hydrogen Energy*, 2012, **37**, 9202-9211.
- 39 V. Baglio, A. S. Arico, A. Di Blasi, P. L. Antonucci, F. Nannetti, V. Tricoli, V. Antonucci, *Journal of Applied Electrochemistry*, 2005, **35**, 207-212.
- 40 X. Li, E. P. L. Roberts, S. M. Holmes, V. Zhobenko, *Solid State Ionics*, 2007, **178**, 1248-1255.
- 41 G. Alberti, M. Casciola, *Annual Review of Materials Research*, 2003, **33**, 129-154.
- 42 H. Tang, Z. Wan, M. Pan, S. P. Jiang, *Electrochemistry Communications*, 2007, **9**, 2003-2008.
- 43 R. H. He, Q. F. Li, G. Xiao, N. J. Bjerrum, *Journal of Membrane Science*, 2003, **226**, 169-184.
- 44 L. Xiao, H. Zhang, T. Jana, E. Scanlon, R. Chen, E. W. Choe, L. S. Ramanathan, S. Yu, B. C. Benicewicz, *Fuel Cells*, 2005, **5**, 287-295.
- 45 L. X. Xiao, H. F. Zhang, E. Scanlon, L. S. Ramanathan, E. W. Choe, D. Rogers, T. Apple, B. C. Benicewicz, *Chemistry of Materials*, 2005, **17**, 5328-5333.
- 46 O. Savadogo, B. Xing, *Journal of New Materials for Electrochemical Systems*, 2000, **3**, 343-347.
- 47 Q. Li, C. Pan, J. O. Jensen, P. Noye, N. J. Bjerrum, *Chemistry of Materials*, 2007, **19**, 350-352.
- 48 W. Zhou, A. S. Bondarenko, B. A. Boukamp, H. J. M. Bouwmeester, *Solid State Ionics*, 2008, **179**, 380-384.
- 49 D. A. Boysen, S. M. Haile, H. J. Liu, R. A. Secco, *Chemistry of Materials*, 2003, **15**, 727-736.
- 50 R. B. Merle, C. R. I. Chisholm, D. A. Boysen, S. M. Haile, *Energy & Fuels*, 2003, **17**, 210-215.
- 51 Y. Yamane, K. Yamada, K. Inoue, *Solid State Ionics*, 2008, **179**, 483-488.
- 52 M. Cappadonia, O. Niemzig, U. Stimming, *Solid State Ionics*, 1999, **125**, 333-337.
- 53 C. Sun, U. Stimming, *Electrochimica Acta*, 2008, **53**, 6417-6422.
- 54 P. Heo, H. Shibata, M. Nagao, T. Hibino, *Solid State Ionics*, 2008, **179**, 1446-1449.
- 55 Y. J. Huang, Q. F. Li, T. V. Anfimova, E. Christensen, M. Yin, J. O. Jensen, N. J. Bjerrum, W. Xing, *International Journal of Hydrogen Energy*, 2013, **38**, 2464-2470.
- 56 A. Goni-Urtiaga, D. Presvytes, K. Scott, *International Journal of Hydrogen Energy*, 2012,

- 37**, 3358-3372.
- 57 S. J. Peighambaroust, S. Rowshanzamir, M. Amjadi, *International Journal of Hydrogen Energy*, 2010, **35**, 9349-9384.
- 58 S. Bose, T. Kuila, X. L. N. Thi, N. H. Kim, K. T. Lau, J. H. Lee, *Progress in Polymer Science*, 2011, **36**, 813-843.
- 59 J. A. Asensio, E. M. Sanchez, P. Gomez-Romero, *Chemical Society Reviews*, 2010, **39**, 3210-3239.
- 60 L. Wu, Z. H. Zhang, J. Ran, D. Zhou, C. R. Li, T. W. Xu, *Physical Chemistry Chemical Physics*, 2013, **15**, 4870-4887.
- 61 W. Y. Dong, Y. J. Sun, C. W. Lee, W. M. Hua, L. X. C., Y. F. Shi, S. C. Zhang, J. M. Chen, D. Y. Zhao, *J Am Chem Soc*, 2007, **129**, 13894-13904.
- 62 F. M. Vichi, M. I. Tejedor-Tejedor, M. A. Anderson, *Chemistry of Materials*, 2000, **12**, 1762-1770.
- 63 F. M. Vichi, M. T. Colomer, M. A. Anderson, *Electrochemical and Solid State Letters*, 1999, **2**, 313-316.
- 64 T. Kasuga, *Thin Solid Films*, 2006, **496**, 141-145.
- 65 H. Ekstrom, B. Wickman, M. Gustavsson, P. Hanarp, L. Eurenus, E. Olsson, G. Lindbergh, *Electrochimica Acta*, 2007, **52**, 4239-4245.
- 66 A. Thorne, A. Kruth, D. Tunstall, J. T. S. Irvine, W. Z. Zhou, *Journal of Physical Chemistry B*, 2005, **109**, 5439-5444.
- 67 E. K. Andersen, J. G. K. Andersen, E. Skou, *Solid State Ionics*, 1988, **27**, 181-187.
- 68 T. Bredow, K. Jug, *Surface Science*, 1995, **327**, 398-408.
- 69 M. I. Tejedor-Tejedor, F. M. Vichi, M. A. Anderson, *Journal of Porous Materials*, 2005, **12**, 201-214.
- 70 M. T. Colomer, *Advanced Materials*, 2006, **18**, 371-+.
- 71 T. Tsuru, Y. Yagi, Y. Kinoshita, M. Asada, *Solid State Ionics*, 2003, **158**, 343-350.
- 72 Y. Jun, H. Zarrin, M. Fowler, Z. W. Chen, *International Journal of Hydrogen Energy*, 2011, **36**, 6073-6081.
- 73 A. Kaithwas, M. Prasad, A. Kulshreshtha, S. Verma, *Chemical Engineering Research & Design*, 2012, **90**, 1632-1641.
- 74 J. J. Zhu, T. Wang, X. L. Xu, P. Xiao, J. L. Li, *Applied Catalysis B-Environmental*, 2013, **130**, 197-217.
- 75 H. B. Li, M. Nogami, *Advanced Materials*, 2002, **14**, 912-914.
- 76 G. L. Athens, Y. Ein-Eli, B. F. Chmelka, *Advanced Materials*, 2007, **19**, 2580-+.
- 77 M. Yamada, D. L. Li, I. Honma, H. S. Zhou, *Journal of the American Chemical Society*, 2005, **127**, 13092-13093.
- 78 Y. Daiko, T. Kasuga, M. Nogami, *Chemistry of Materials*, 2002, **14**, 4624-4627.
- 79 H. B. Li, M. Nogami, *Chemical Communications*, 2003, 236-237.
- 80 T. Uma, M. Nogami, *Chemistry of Materials*, 2007, **19**, 3604-3610.
- 81 L. M. Xiong, M. Nogami, *Chemistry Letters*, 2006, **35**, 972-973.
- 82 J. D. Halla, M. Mamak, D. E. Williams, G. A. Ozin, *Advanced Functional Materials*, 2003, **13**, 133-138.
- 83 S. N. Azizi, S. Ghasemi, E. Chiani, *Electrochimica Acta*, 2013, **88**, 463-472.
- 84 B. Y. Jiang, H. L. Tang, M. Pan, *International Journal of Hydrogen Energy*, 2012, **37**, 4612-4618.
- 85 Y. Ye, C. Jo, I. Jeong, J. Lee, *Nanoscale*, 2013, **5**, 4584-4605.

- 86 J. S. Beck, J. C. Vartuli, W. J. Roth, M. E. Leonowicz, C. T. Kresge, K. D. Schmitt, C. T. W. Chu, D. H. Olson, E. W. Sheppard, S. B. McCullen, J. B. Higgins, J. L. Schlenker, *Journal of the American Chemical Society*, 1992, **114**, 10834-10843.
- 87 C. T. Kresge, M. E. Leonowicz, W. J. Roth, J. C. Vartuli, J. S. Beck, *Nature*, 1992, **359**, 710-712.
- 88 Y. Wan, D. Y. Zhao, *Chemical Reviews*, 2007, **107**, 2821-2860.
- 89 H. B. Li, T. Kunitake, *Microporous and Mesoporous Materials*, 2006, **97**, 42-48.
- 90 M. T. Colomer, F. Rubio, J. R. Jurado, *Journal of Power Sources*, 2007, **167**, 53-57.
- 91 M. Nogami, R. Nagao, C. Wong, *Journal of Physical Chemistry B*, 1998, **102**, 5772-5775.
- 92 M. Nogami, Y. Abe, *Physical Review B*, 1997, **55**, 12108-12112.
- 93 Y. Daiko, T. Kasuga, M. Nogami, *Microporous and Mesoporous Materials*, 2004, **69**, 149-155.
- 94 M. Sharifi, R. Marschall, M. Wilkening, M. Wark, *Journal of Power Sources*, 2010, **195**, 7781-7786.
- 95 M. Nogami, H. B. Li, Y. Daiko, T. Mitsuoka, *Journal of Sol-Gel Science and Technology*, 2004, **32**, 185-188.
- 96 H. B. Li, D. L. Jin, X. Y. Kong, H. Y. Tu, Q. C. Yu, F. J. Jiang, *Microporous and Mesoporous Materials*, 2011, **138**, 63-67.
- 97 R. Marschall, I. Bannat, A. Feldhoff, L. Z. Wang, G. Q. Lu, M. Wark, *Small*, 2009, **5**, 854-859.
- 98 M. T. Colomer, M. A. Anderson, *Journal of Non-Crystalline Solids*, 2001, **290**, 93-104.
- 99 S. Suzuki, Y. Nozaki, T. Okumura, M. Miyayama, *Journal of the Ceramic Society of Japan*, 2006, **114**, 303-307.
- 100 M. Nogami, R. Nagao, G. Wong, T. Kasuga, T. Hayakawa, *Journal of Physical Chemistry B*, 1999, **103**, 9468-9472.
- 101 M. Nogami, Y. Goto, Y. Tsurita, T. Kasuga, *Journal of the American Ceramic Society*, 2001, **84**, 2553-2556.
- 102 C. Wang, M. Nogami, *Materials Letters*, 2000, **42**, 225-228.
- 103 S. P. Tung, B. J. Hwang, *Journal of Materials Chemistry*, 2005, **15**, 3532-3538.
- 104 S. Mikhailenko, D. Desplandier-Giscard, C. Danumah, S. Kaliaguine, *Microporous and Mesoporous Materials*, 2002, **52**, 29-37.
- 105 D. Margolese, J. A. Melero, S. C. Christiansen, B. F. Chmelka, G. D. Stucky, *Chemistry of Materials*, 2000, **12**, 2448-2459.
- 106 R. Marschall, J. Rathousky, M. Wark, *Chemistry of Materials*, 2007, **19**, 6401-6407.
- 107 R. Marschall, I. Bannat, J. Caro, M. Wark, *Microporous and Mesoporous Materials*, 2007, **99**, 190-196.
- 108 R. Supplit, A. Sugawara, H. Peterlik, R. Kikuchi, T. Okubo, *European Journal of Inorganic Chemistry*, 2010, 3993-3999.
- 109 T. Ioroi, K. Kuraoka, K. Yasuda, T. Yazawa, Y. Miyazaki, *Electrochemical and Solid State Letters*, 2004, **7**, A394-A396.
- 110 A. Matsuda, T. Kanzaki, K. Tadanaga, T. Kogure, M. Tatsumisago, T. Minami, *Journal of the Electrochemical Society*, 2002, **149**, E292-E297.
- 111 R. Marschall, M. Sharifi, M. Wark, *Microporous and Mesoporous Materials*, 2009, **123**, 21-29.
- 112 Y. G. Jin, S. Z. Qiao, Z. P. Xu, J. C. D. da Costa, G. Q. Lu, *Journal of Physical Chemistry C*, 2009, **113**, 3157-3163.

- 113 Y. G. Jin, S. Z. Qiao, Z. P. Xu, Z. M. Yan, Y. N. Huang, J. C. D. da Costa, G. Q. Lu, *Journal of Materials Chemistry*, 2009, **19**, 2363-2372.
- 114 V. G. Ponomareva, E. S. Shutova, *Solid State Ionics*, 2005, **176**, 2905-2908.
- 115 V. G. Ponomareva, E. S. Shutova, *Solid State Ionics*, 2007, **178**, 729-734.
- 116 M. Nogami, R. Nagao, C. Wong, T. Kasuga, T. Hayakawa, *The Journal of Physical Chemistry B*, 1999, **103**, 9468-9472.
- 117 M. Nogami, Y. Daiko, T. Akai, T. Kasuga, *J. Phys. Chem. B*, 2001, **105**, 4653-4656.
- 118 T. Uma, M. Nogami, *Journal of Membrane Science*, 2008, **323**, 11-16.
- 119 T. Uma, M. Nogami, *Anal. Chem.*, 2008, **80**, 506-508.
- 120 T. Inoue, T. Uma, M. Nogami, *Journal of Membrane Science*, 2008, **323**, 148-152.
- 121 T. Uma, M. Nogami, *Fuel Cells*, 2007, **7**, 279-284.
- 122 T. Uma, M. Nogami, *Chemistry of Materials*, 2007, **19**, 3604-3610.
- 123 T. Uma, M. Nogami, *Journal of The Electrochemical Society*, 2007, **154**, B845-B851.
- 124 T. Uma, M. Nogami, *Journal of Membrane Science*, 2009, **334**, 123-128.
- 125 M. Nogami, H. Matsushita, Y. Goto, T. Kasuga, *Advanced Materials*, 2000, **12**, 1370-1372.
- 126 T. Uma, M. Nogami, *Analytical Chemistry*, 2008, **80**, 506-508.
- 127 M. Nogami, K. Tanaka, T. Uma, *Fuel Cells*, 2009, **9**, 528-533.
- 128 N. Nakamoto, A. Matsuda, K. Tadanaga, T. Minami, M. Tatsumisago, *Journal of Power Sources*, 2004, **138**, 51-55.
- 129 T. Ishiyama, S. Suzuki, J. Nishii, T. Yamashita, H. Kawazoe, T. Omata, *Journal of the Electrochemical Society*, 2013, **160**, E143-E147.
- 130 Z. G. Di, H. B. Li, M. Li, D. L. Mao, X. J. Chen, M. Xiao, J. Gu, *Journal of Power Sources*, 2012, **207**, 86-90.
- 131 H. Shen, H. Maekawa, J. Kawamura, Y. Matsumoto, T. Yamamura, Y. Kawakita, K. Shibata, M. Kawai, *Solid State Ionics*, 2008, **179**, 1133-1137.
- 132 H. Y. Shen, H. Maekawa, J. Kawamura, T. Yamamura, *Solid State Ionics*, 2006, **177**, 2403-2406.
- 133 H. Shen, H. Maekawa, L. Wang, B. Guo, K. Y. Shu, *Electrochemical and Solid State Letters*, 2009, **12**, B18-B21.
- 134 M. T. Colomer, *Journal of Power Sources*, 2011, **196**, 8280-8285.
- 135 M. T. Colomer, K. Zenzinger, *Microporous and Mesoporous Materials*, 2012, **161**, 123-133.
- 136 S. Escolastico, C. Solis, J. M. Serra, *International Journal of Hydrogen Energy*, 2011, **36**, 11946-11954.
- 137 E. M. Tsui, M. M. Cortalezzi, M. R. Wiesner, *Journal of Membrane Science*, 2007, **306**, 8-15.
- 138 L. W. Zhang, S. R. Chae, Z. Hendren, J. S. Park, M. R. Wiesner, *Chemical Engineering Journal*, 2012, **204**, 87-97.
- 139 F. M. Gao, J. L. He, E. D. Wu, S. M. Liu, D. L. Yu, D. C. Li, S. Y. Zhang, Y. J. Tian, *Physical Review Letters*, 2003, **91**.
- 140 H. L. Tang, M. Pan, S. F. Lu, J. L. Lu, S. P. Jiang, *Chemical Communications*, 2010, **46**, 4351-4353.
- 141 S. P. Jiang, *Solid State Ionics*, 2013, in press.
- 142 M. Amirinejad, S. S. Madaeni, E. Rafiee, S. Amirinejad, *Journal of Membrane Science*, 2011, **377**, 89-98.

- 143 O. Nakamura, T. Kodama, I. Ogino, Y. Miyake, *Chemistry Letters*, 1979, 17-18.
- 144 D. L. Wang, S. F. Lu, S. P. Jiang, *Chemical Communications*, 2010, **46**, 2058-2060.
- 145 Y. Xiang, M. Yang, J. Zhang, F. Lan, S. F. Lu, *Journal of Membrane Science*, 2011, **368**, 241-245.
- 146 T. Kukino, R. Kikuchi, T. Takeguchi, T. Matsui, K. Eguchi, *Solid State Ionics*, 2005, **176**, 1845-1848.
- 147 Z. M. Cui, W. Xing, C. P. Liu, D. Tian, H. Zhang, *Journal of Power Sources*, 2010, **195**, 1619-1623.
- 148 J. Zeng, S. P. Jiang, *Journal of Physical Chemistry C*, 2011, **115**, 11854-11863.
- 149 L. Mercier, T. J. Pinnavaia, *Advanced Materials*, 1997, **9**, 500-&.
- 150 A. Cauvel, G. Renard, D. Brunel, *Journal of Organic Chemistry*, 1997, **62**, 749-751.
- 151 R. J. P. Corriu, C. Hoarau, A. Mehdi, C. Reye, *Chemical Communications*, 2000, 71-72.
- 152 D. J. Macquarrie, *Chemical Communications*, 1996, 1961-1962.
- 153 N. Bibent, A. Mehdi, G. Silly, F. Henn, S. Devautour-Vinot, *European Journal of Inorganic Chemistry*, 2011, 3214-3225.
- 154 A. Pettersson, J. B. Rosenholm, *Langmuir*, 2002, **18**, 8447-8454.
- 155 J. L. Lu, H. L. Tang, S. F. Lu, H. W. Wu, S. P. Jiang, *Journal of Materials Chemistry*, 2011, **21**, 6668-6676.
- 156 P. M. Rao, P. Goldberg-Opppenheimer, S. Kababya, S. Vega, M. Landau, *Journal of Molecular Catalysis a-Chemical*, 2007, **275**, 214-227.
- 157 J. Zeng, Y. H. Zhou, L. Li, S. P. Jiang, *Physical Chemistry Chemical Physics*, 2011, **13**, 10249-10257.
- 158 J. Zeng, P. K. Shen, S. F. Lu, Y. Xiang, L. Li, R. De Marco, S. P. Jiang, *Journal of Membrane Science*, 2012, **397**, 92-101.
- 159 R. Fan, S. Huh, R. Yan, J. Arnold, P. D. Yang, *Nature Materials*, 2008, **7**, 303-307.
- 160 Y. S. Ye, W. Y. Chen, Y. J. Huang, M. Y. Cheng, Y. C. Yen, C. C. Cheng, F. C. Chang, *Journal of Membrane Science*, 2010, **362**, 29-37.
- 161 X. M. Yan, P. Mei, Y. Z. Mi, L. Gao, S. X. Qin, *Electrochemistry Communications*, 2009, **11**, 71-74.
- 162 H. L. Tang, M. Pan, S. P. Jiang, *Dalton Transactions*, 2011, **40**, 5220-5227.
- 163 F. Lefebvre, *Journal of the Chemical Society-Chemical Communications*, 1992, 756-757.
- 164 S. C. Thomas, X. M. Ren, S. Gottesfeld, P. Zelenay, *Electrochimica Acta*, 2002, **47**, 3741-3748.
- 165 S. Wasmus, A. Kuver, *Journal of Electroanalytical Chemistry*, 1999, **461**, 14-31.
- 166 E. A. Cho, U. S. Jeon, S. A. Hong, I. H. Oh, S. G. Kang, *Journal of Power Sources*, 2005, **142**, 177-183.
- 167 F. Alcaide, G. Alvarez, J. A. Blazquez, P. L. Cabot, O. Miguel, *International Journal of Hydrogen Energy*, 2010, **35**, 5521-5527.
- 168 S. Siracusano, V. Baglio, A. Di Blasi, N. Briguglio, A. Stassi, R. Ornelas, E. Trifoni, V. Antonucci, A. S. Arico, *International Journal of Hydrogen Energy*, 2010, **35**, 5558-5568.
- 169 D. Thirumalai, R. E. White, *Journal of the Electrochemical Society*, 1997, **144**, 1717-1723.
- 170 F. B. Weng, B. S. Jou, A. Su, S. H. Chan, P. H. Chi, *Journal of Power Sources*, 2007, **171**, 179-185.
- 171 J. Zeng, B. Jin, P. K. Shen, B. He, K. Lamb, R. De Marco, S. P. Jiang, *International Journal of Hydrogen Energy*, 2013, **38**, 12830-12837.
- 172 M. Nagao, A. Takeuchi, P. Heo, T. Hibino, M. Sano, A. Tomitab, *Electrochemical and*

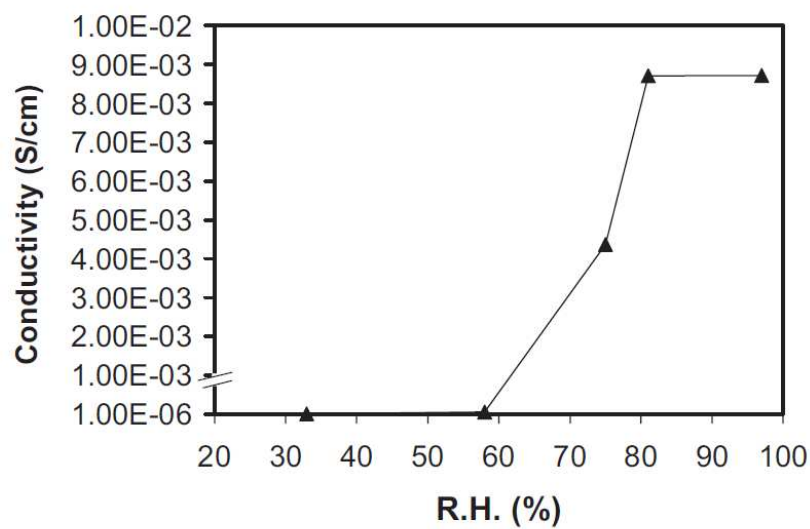
- Solid State Letters*, 2006, **9**, A105-A109.
- 173 D. A. Boysen, T. Uda, C. R. I. Chisholm, S. M. Haile, *Science*, 2004, **303**, 68-70.
- 174 J. Zeng, B. He, K. Lamb, R. De Marco, P. K. Shen, S. P. Jiang, *Chemical communications (Cambridge, England)*, 2013, **49**, 4655-7.
- 175 J. Zeng, B. He, K. Lamb, R. De Marco, P. K. Shen, S. P. Jiang, *Acs Applied Materials & Interfaces*, 2013, **5**, 11240-11248.
- 176 T. Tezuka, K. Tadanaga, A. Matsuda, A. Hayashi, M. Tatsumisago, *Solid State Ionics*, 2005, **176**, 3001-3004.
- 177 Y. Z. Li, E. Muto, Y. Aoki, T. Kunitake, *Journal of the Electrochemical Society*, 2010, **157**, B1103-B1108.
- 178 A. K. Mishra, T. Kuila, D. Y. Kim, N. H. Kim, J. H. Lee, *Journal of Materials Chemistry*, 2012, **22**, 24366-24372.
- 179 V. G. Ponomareva, K. A. Kovalenko, A. P. Chupakhin, D. N. Dybtsev, E. S. Shutova, V. P. Fedin, *Journal of the American Chemical Society*, 2012, **134**, 15640-15643.
- 180 S. P. Jiang, *International Journal of Hydrogen Energy*, 2012, **37**, 449-470.

**Table 1.** Properties, conductivities and cell performance of functionalized mesoporous materials based PEMFCs.

Mesoporous materials	Dopant or functionalization	Properties			Notes	Ref
		BET, pore size/nm	Conductivity	Cell performance		
zirconium phosphates	None	177 m <sup>2</sup> /g, 2-4 nm	4.1×10 <sup>-6</sup> S/cm, 22°C, 84%RH	n.a.	σ is sensitive to RH.	37
α-Fe <sub>2</sub> O <sub>3</sub>		239 m <sup>2</sup> /g, 3.8 nm	9.06×10 <sup>-4</sup> S/cm, 40°C, 81%RH	n.a.	Highest temp reported: 90°C	135
FeOOH	None	96 m <sup>2</sup> /g, ~25 nm	0.02 S/cm, 25°C, 100%RH	n.a.	Plate-like particles	137
Al <sub>2</sub> O <sub>3</sub>	none	43.1 m <sup>2</sup> /g, 10.2 nm	4.0×10 <sup>-3</sup> S/cm, 25°C, 90%RH	n.a.		131, 132
Al <sub>2</sub> O <sub>3</sub>	LaCl <sub>3</sub>		3.0×10 <sup>-2</sup> S/cm, 25°C, 90%RH	n.a.		133
TiO <sub>2</sub>	None	134 m <sup>2</sup> /g, ~5 nm	0.01 S/cm, 25°C, 81%RH	n.a.	σ is sensitive to RH.	62
TiO <sub>2</sub>	Phosphate	134 m <sup>2</sup> /g, ~5 nm	9.7×10 <sup>-3</sup> S/cm, 25°C, pH 2.5	n.a.		62
TiO <sub>2</sub> nanotubes	None		5.5×10 <sup>-6</sup> S/cm, 27°C, 70%RH	n.a.	Not stable above 150°C	66
Si-MCM-41	none	1030 m <sup>2</sup> /g, 2.7 nm	1×10 <sup>-6</sup> S/cm, 140°C, 100%RH	n.a.		106
5%P <sub>2</sub> O <sub>5</sub> -95%SiO <sub>2</sub>	5% P <sub>2</sub> O <sub>5</sub>	631 m <sup>2</sup> /g, 2 nm	1.3×10 <sup>-2</sup> S/cm, 80°C, 80%RH	70.3 mW/cm <sup>2</sup> at 80°C, 75% RH, H <sub>2</sub> /O <sub>2</sub> .	10wt% H <sub>3</sub> PO <sub>4</sub> was used as binder	127
5%P <sub>2</sub> O <sub>5</sub> -95%SiO <sub>2</sub>	5% P <sub>2</sub> O <sub>5</sub>	631 m <sup>2</sup> /g, 2 nm	1.0×10 <sup>-3</sup> S/cm, 80°C, 80%RH	28.3 mW/cm <sup>2</sup> at 80°C, 75% RH, H <sub>2</sub> /O <sub>2</sub> .	10wt% PTFE was used as binder	127
ZrO <sub>2</sub> -P <sub>2</sub> O <sub>5</sub> -SiO <sub>2</sub>	HPM	~350 m <sup>2</sup> /g, 2.4 nm	10 <sup>-3</sup> -10 <sup>-1</sup> S/cm, 30-90 °C, 80%RH	32 mW/cm <sup>2</sup> at 29°C, 30% RH, H <sub>2</sub> /O <sub>2</sub> .	Active cell area: 0.25 cm <sup>2</sup>	124
P <sub>2</sub> O <sub>5</sub> -SiO <sub>2</sub> /Nafion	None			207 mW/cm <sup>2</sup> at 70°C, humidified, H <sub>2</sub> /O <sub>2</sub> .	Nafion layer: 800 nm	130
Si-MCM-41	-SO <sub>3</sub> H	1030 m <sup>2</sup> /g, 2.7 nm	0.2 S/cm, 140°C, 100%RH	n.a.	σ is sensitive to RH.	106
Si-MCM-41	H <sub>3</sub> PO <sub>4</sub>	~950 m <sup>2</sup> /g, ~2.0 nm	0.015 S/cm, 130°C, 100%RH	n.a.	σ is sensitive to RH.	112
Si-MCM-41	HPW	~3.0 nm	0.045 S/cm, 150°C, 100%RH	95 mW/cm <sup>2</sup> at 100°C, 100%RH, H <sub>2</sub> /O <sub>2</sub> . 90 mW/cm <sup>2</sup> at 150°C, 1%RH, CH <sub>3</sub> OH/O <sub>2</sub> .	Membrane thickness: 0.8 mm.	28
SiO <sub>2</sub>	HPW	~950 m <sup>2</sup> /g, 5-8 nm	0.076 S/cm, 100°C, 100%RH; 0.05 S/cm, 200°C, 0%RH.	128.5 mW/cm <sup>2</sup> at 200°C, 112 mW/cm <sup>2</sup> at 200°C,	Membrane thickness: 0.16 mm; active area: 4 cm <sup>2</sup> .	157, 162

				$\text{CH}_3\text{CH}_2\text{OH}/\text{O}_2$ .		
$\text{SiO}_2$	HPW		0.13 S/cm, 100°C, 100%RH;	74.4 W at 150°C in $\text{H}_2/\text{O}_2$ .	10-cell stack; membrane thickness: 0.75mm; active area: 200 cm <sup>2</sup>	<sup>171</sup>
$\text{SiO}_2$ , sintered at 650°C	$\text{H}_3\text{PO}_4$	948 m <sup>2</sup> /g, 8.2 nm	0.04 S/cm, 200°C, 0%RH;	570 mW/cm <sup>2</sup> at 190°C, 0% RH, & 700 mW/cm <sup>2</sup> at 190°C, 3% RH, $\text{H}_2/\text{O}_2$ .	Membrane thickness: 0.5 mm.	<sup>174</sup> , <sup>175</sup>



**Figures and Captions:**

**Figure 1.** Proton conductivity of the calcined anatase thin films measured at room temperature under different RH conditions.<sup>70</sup>

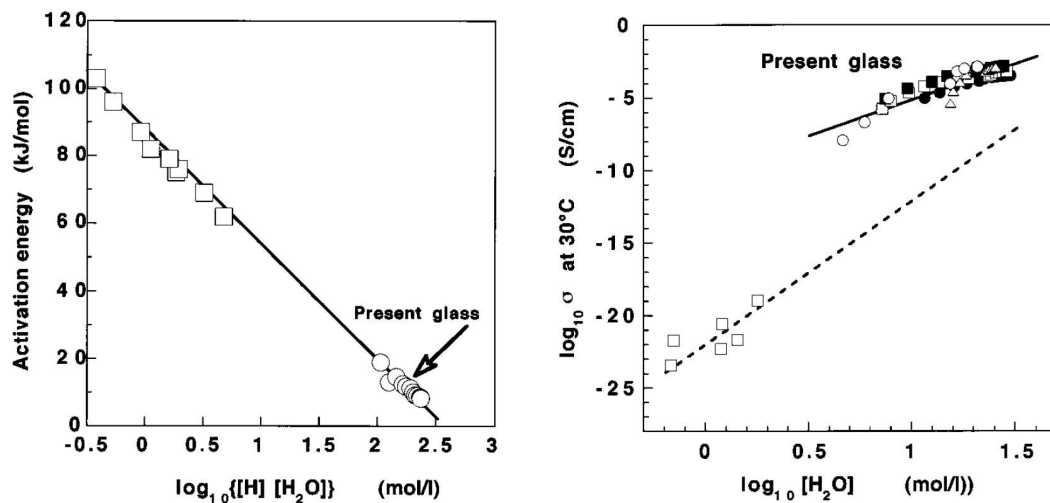


**Figure 2.** (a) Relationship between activation energy for conduction and concentration of protons and water, and (b) relationship between the conductivity and logarithm of concentration of water.<sup>91</sup>

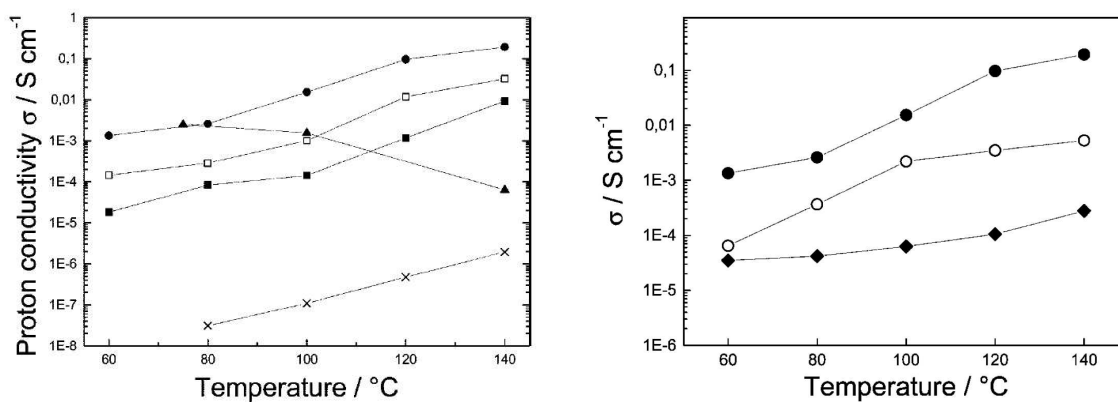


**Figure 3.** Proton conductivity measured (a) at 100% RH for 0% ( $\times$ ), 20% ( $\blacksquare$ ), 30% ( $\square$ ), and 40% ( $\bullet$ )  $\text{SO}_3\text{H-MCM-41}$  and for Nafion ( $\blacktriangle$ ) and (b) on 40%  $\text{SO}_3\text{H-MCM-41}$  at 0% ( $\blacklozenge$ ), 50% ( $\circ$ ) and 100% ( $\bullet$ ) RH.<sup>106</sup>

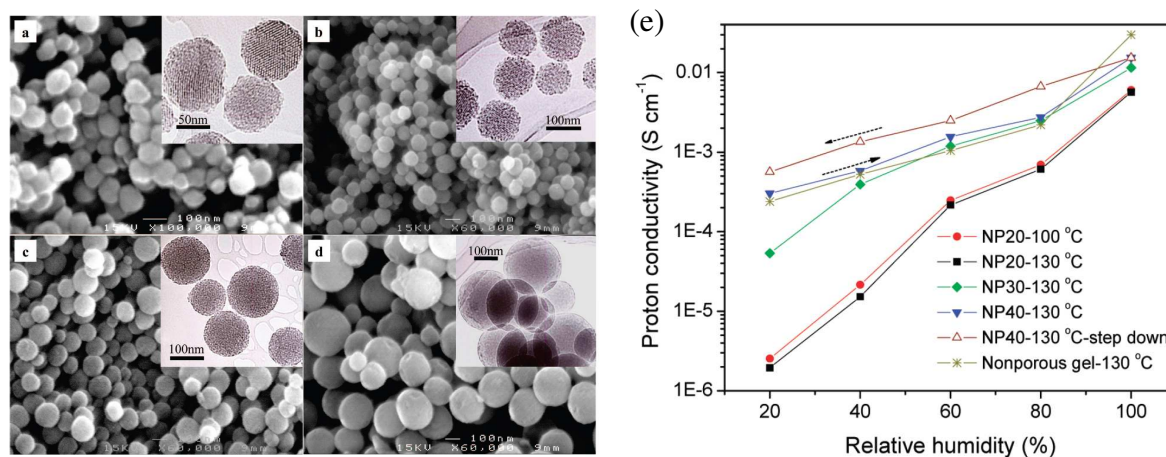


**Figure 4.** SEM and TEM (inset) images of (a) NP10, (b) NP20, (c) NP30, and (d) NP40, where NP10, NP20, NP30, and NP40 stands for the nominal P/Si molar ratio of 10%, 20%, 30% and 40% in the acidified product, respectively, (e) proton conductivity of phosphonic acid functionalized silica nanospheres as a function of RH at 100 and 130°C.<sup>112</sup>

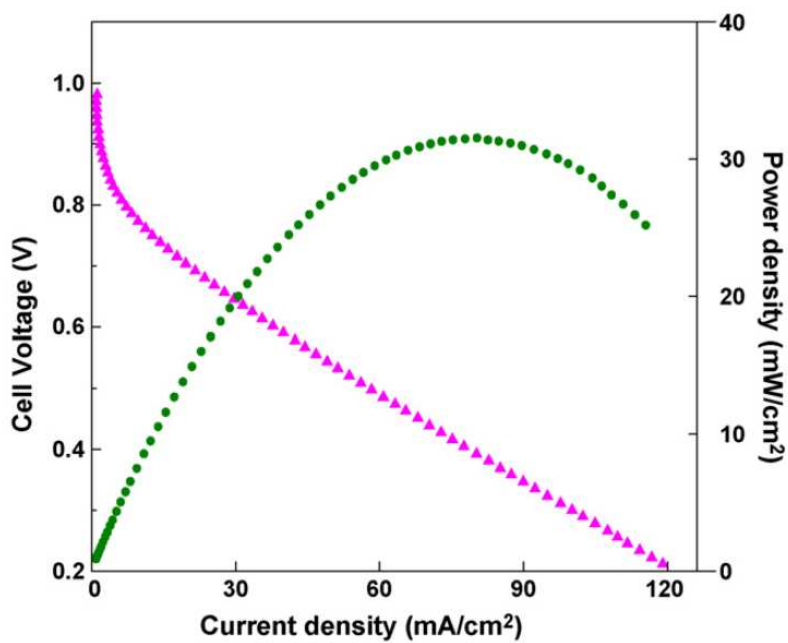


**Figure 5.** The H<sub>2</sub>/O<sub>2</sub> fuel cell performance of the HPMo/ZrO<sub>2</sub>-P<sub>2</sub>O<sub>5</sub>-SiO<sub>2</sub> (2/4-4-90 mol%) glass composite membrane at 29°C and 30% RH.<sup>124</sup>

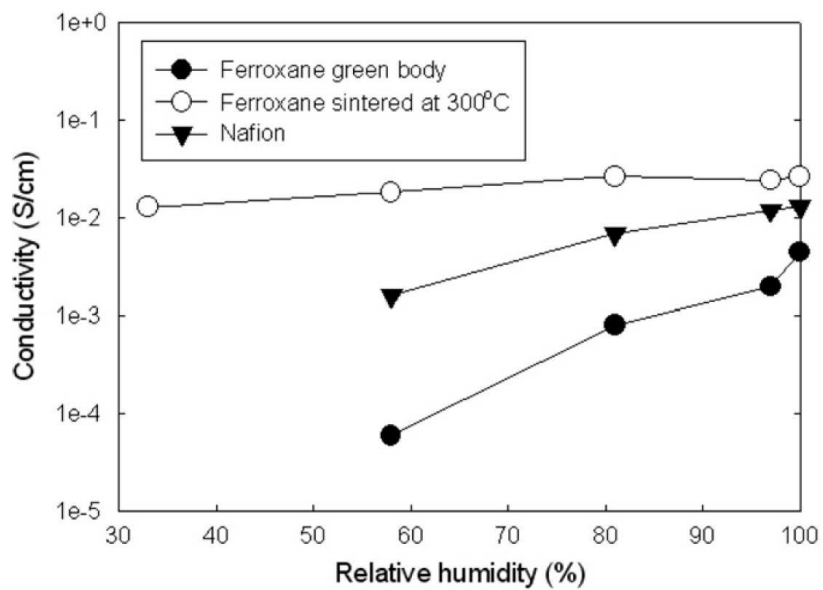


**Figure 6.** Plots of proton conductivity of ferroxane green body, ferroxane sintered at 300 °C and Nafion at different humidities. The tests were conducted at room temperature.<sup>138</sup>

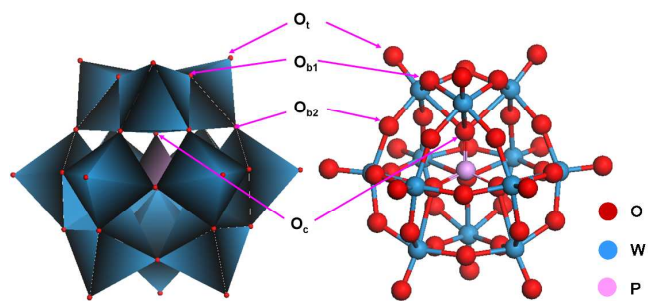


**Figure 7.** The Keggin structure of anion phosphotungstic acid ( $\text{PW}_{12}\text{O}_{40}^{3-}$ ):  $\text{O}_t$ ,  $\text{O}_{b1}$ ,  $\text{O}_{b2}$ , and  $\text{O}_c$  labeled the four types of oxygen in the structure (oxygen atoms in red; tungsten in cyan; phosphor in magenta).

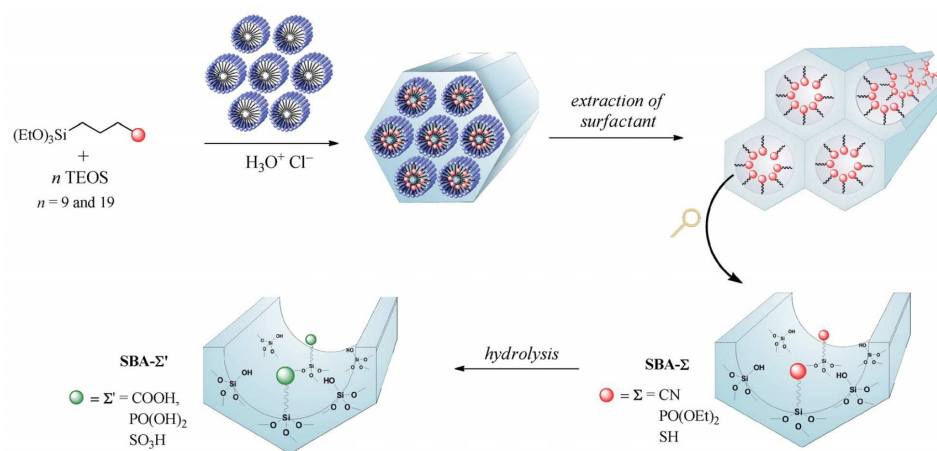


**Figure 8.** The synthesis of the acid-functionalized mesoporous silica, SBA-CO<sub>2</sub>H, SBA-PO(OH)<sub>2</sub> and SBA-SO<sub>3</sub>H.<sup>153</sup>



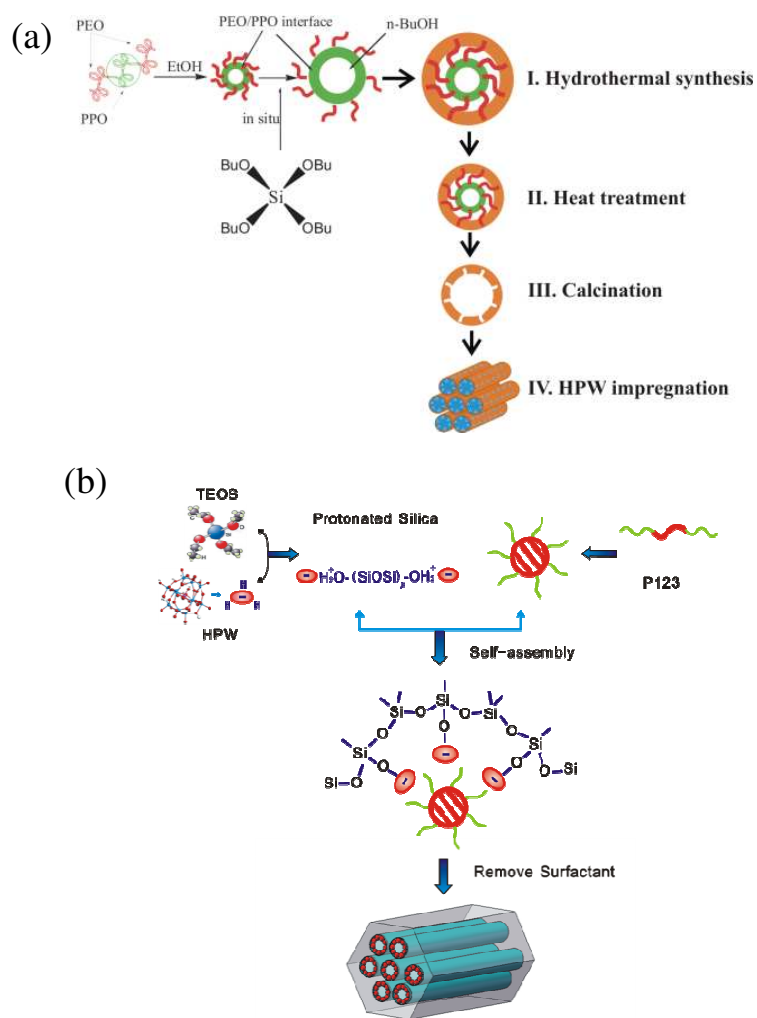


**Figure 9.** Schematic of synthesis of HPW-meso-silica via (a) two-step HPW impregnation process and (b) one-step self-assembly process.<sup>148, 155</sup>

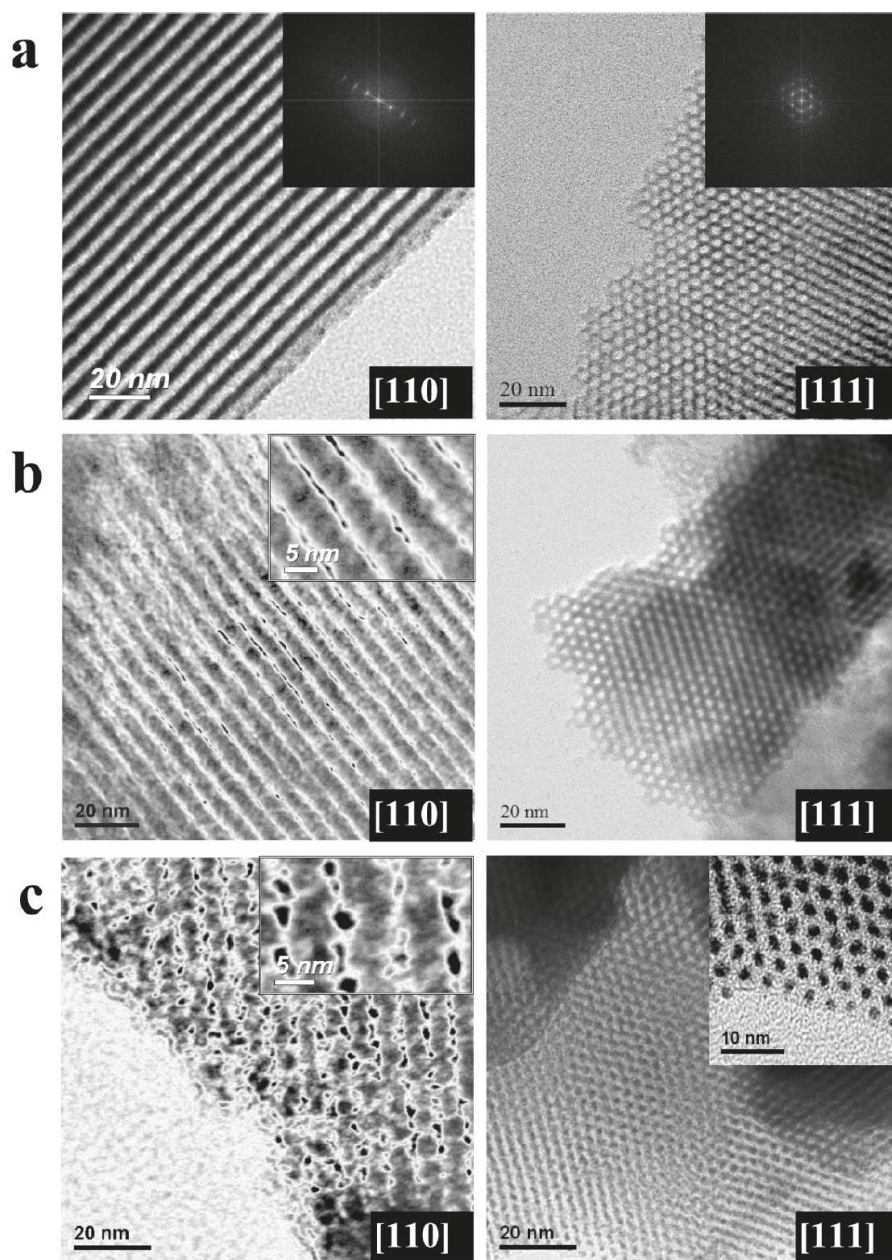


**Figure 10.** TEM images of (a) pure meso-silica and (b) 20% and (c) 80% HPW-meso-silica. The left images were viewed from the [110] direction, whereas the right images were viewed from the [111] direction.<sup>148</sup>

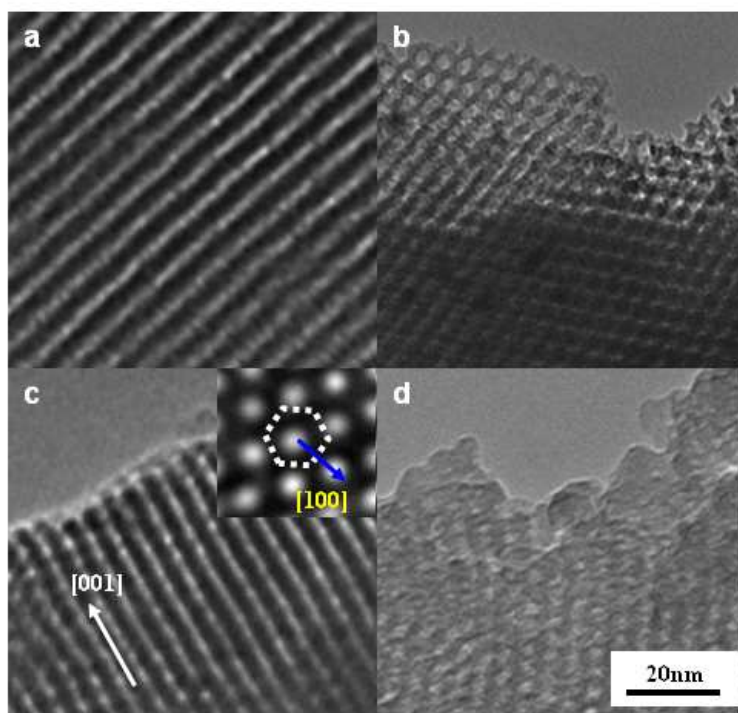


**Figure 11.** TEM micrographs of (a) pure SBA-15 silica; (b) 5wt% HPW-meso-silica; (c) 25wt% HPW-meso-silica and (d) 35wt% HPW-meso-silica. The inset in (c) is the TEM image viewing along the pore axis. The scale bar applies to all TEM micrographs.<sup>155</sup>

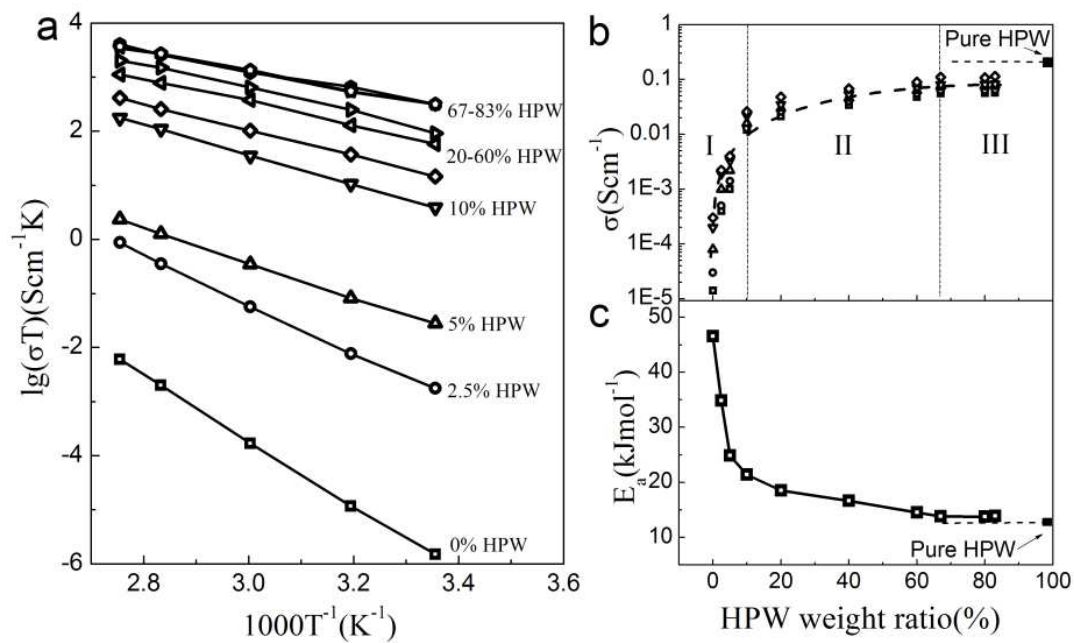


**Figure 12.** (a) Proton conductivity versus temperature of the HPW-meso-silica composite membranes as a function of HPW contents, (b) Proton conductivity versus HPW content measured at 25°C, and (c) Activation energy versus HPW content of HPW-meso-silica membrane.<sup>148</sup>

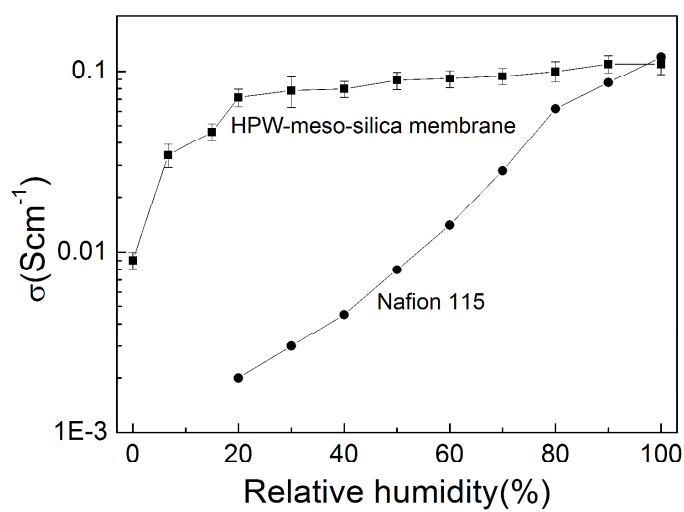


**Figure 13.** The conductivity of a HPW-*meso*-silica nanocomposite measured at 80°C and reference Nafion 115 membrane measured at 30°C as a function of relative humidity.<sup>157</sup>

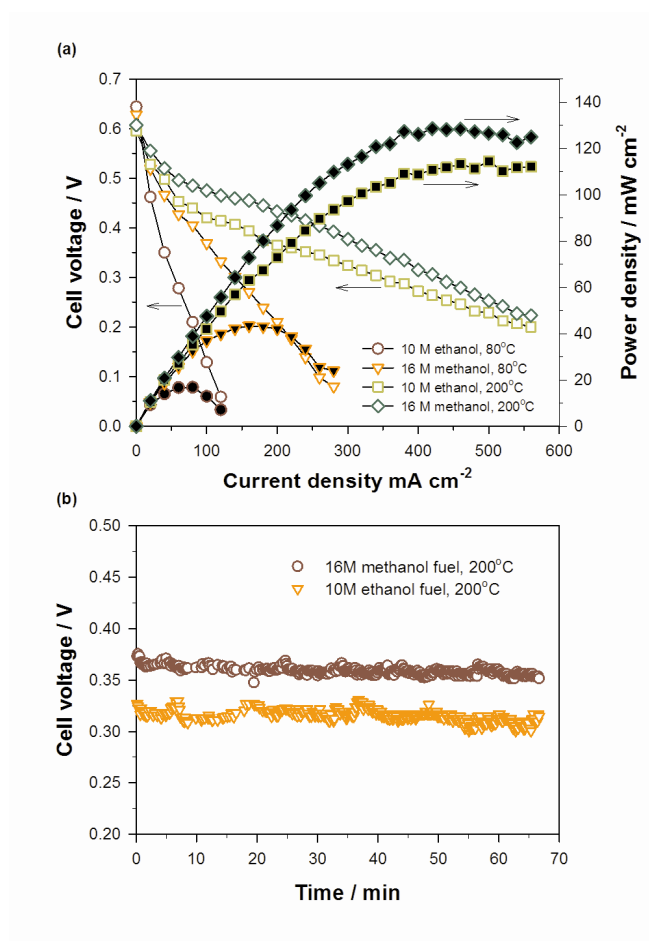


**Figure 14.** Performance and stability of single cells assembled by a 165  $\mu\text{m}$ -thick 25 wt% HPW-*meso*-silica nanocomposite membrane for direct alcohol fuel cells in the absence of external humidification. The stability of the cell was measured at a constant current of  $300 \text{ mA cm}^{-2}$  at  $200^\circ\text{C}$ . Pt black ( $1.0 \text{ mg cm}^{-2}$ ) was used as the anode and cathode electrocatalysts.<sup>162</sup>

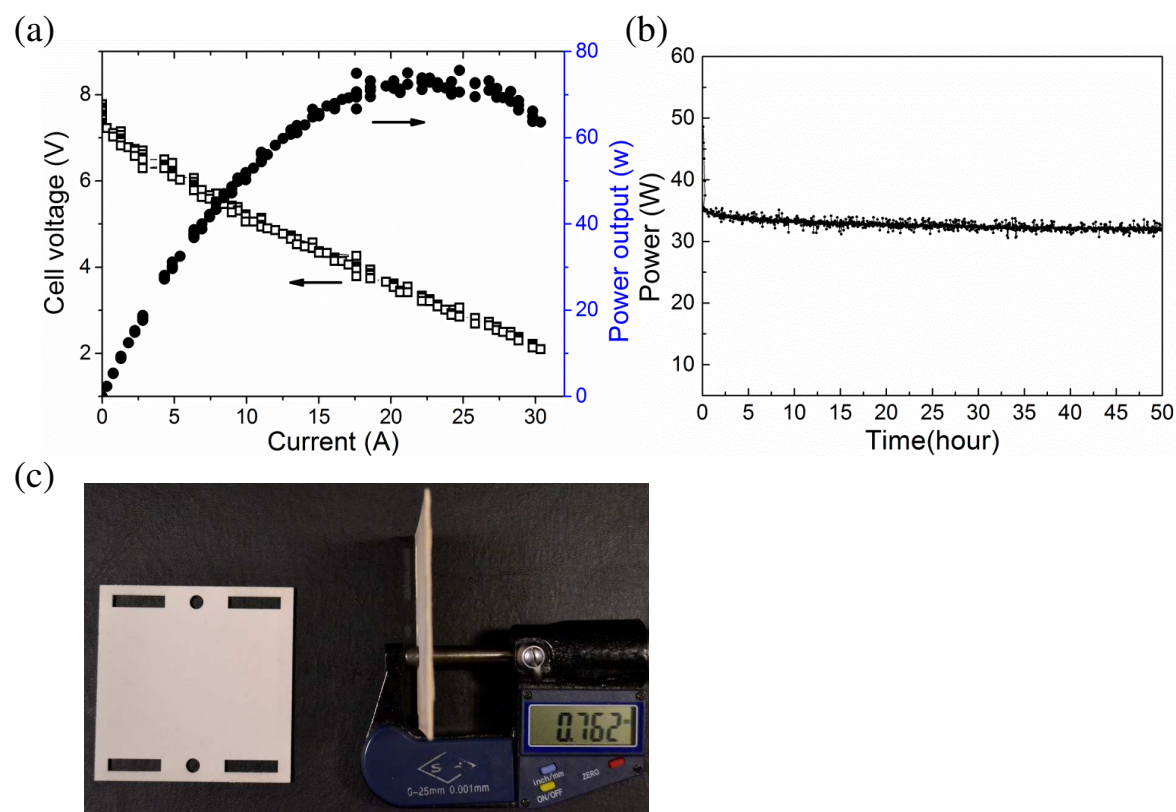


**Figure 15.** (a) Polarization and power density of a 10-cell stack measured in  $\text{H}_2/\text{O}_2$  (1/1 atm) at  $150\text{ }^\circ\text{C}$ ; (b) Stability of a 10-cell stack measured at a stack voltage of 6.0 V and  $150\text{ }^\circ\text{C}$  in  $\text{H}_2/\text{air}$  (1/1 atm). The image in (c) shows a HPW-*meso*-silica membrane with a thickness of  $762\text{ }\mu\text{m}$  and dimension of  $62\text{ mm} \times 62\text{ mm}$ . Note, Pt/C was used as catalyst with a loading of  $0.4\text{ mg cm}^{-2}$  for both anode and cathode, and the effective area of the stack was  $200\text{ cm}^2$ .<sup>171</sup>

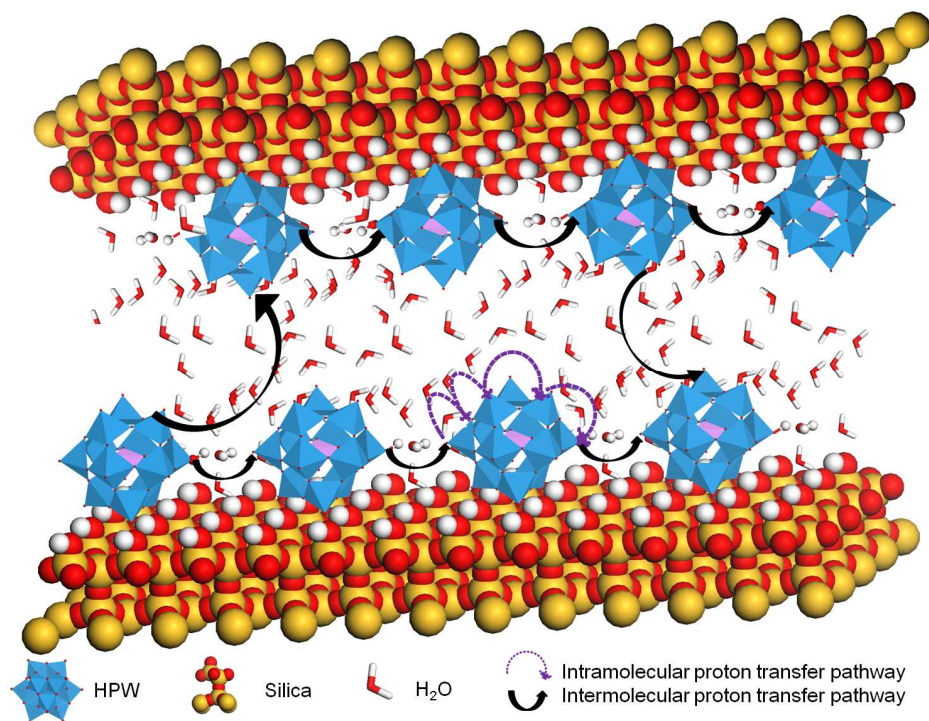


**Figure 16.** The proposed proton transportation in HPW-*meso*-silica nanocomposites via intramolecular and intermolecular proton hopping.



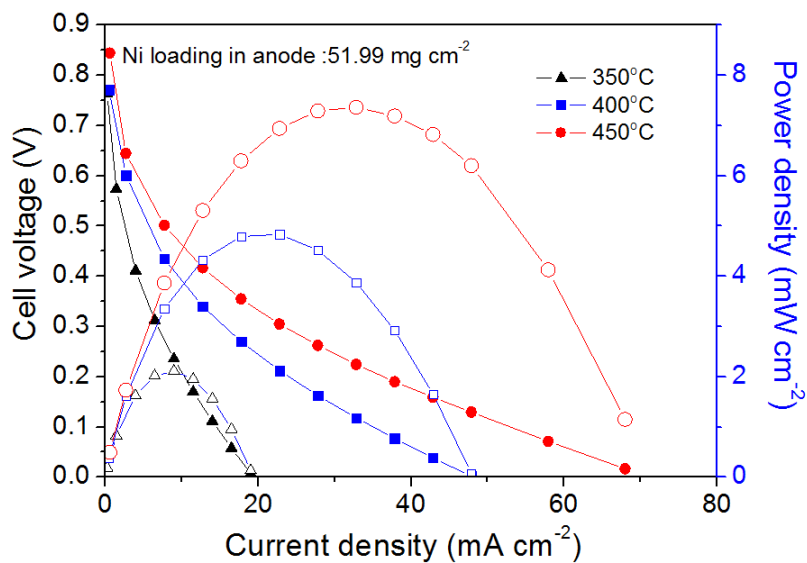


**Figure 17.** Power output of a single cell employing a HPW/sintered *meso*-silica nanocomposite membrane using Ni anode and Pt cathode in  $\text{H}_2/\text{air}$  at different temperatures (unpublished data).